SPACE POWER AND PROPULSION SECTION

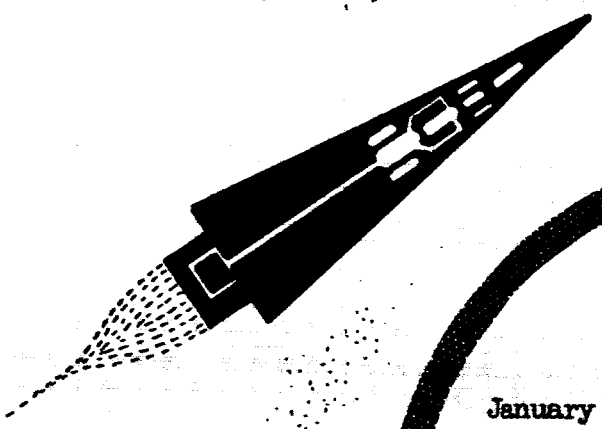

MONTHLY REPORTS

For Periods Ending
January 27, 1964 and February 27, 1964

ELECTROMAGNETIC ALKALI METAL
PUMP RESEARCH PROGRAM

Under Contract NAS 3-2543

For

THE NATIONAL AERONAUTICS
AND SPACE ADMINISTRATION

MISSILE and SPACE DIVISION
GENERAL ELECTRIC
CINCINNATI, OHIO

SPACE POWER AND PROPULSION SECTION

MONTHLY PROJECT STATUS REPORTS

January 27, 1964 and February 27, 1964

ELECTROMAGNETIC ALKALI METAL PUMP RESEARCH PROGRAM

NATIONAL AERONAUTICS AND SPACE ADMININSTRATION

CONTRACT NUMBER NAS 3-2543

RE-ENTRY SYSTEMS DEPARTMENT

GENERAL ELECTRIC COMPANY

CINCINNATI, OHIO 45215

TABLE OF CONTENTS

I. SUMMARY

The Re-Entry Systems Department of the General Electric Company has been under contract to the National Aeronautics and Space Administration since June 27, 1963, for the performance of a research program to study electromagnetic pumps for application to Space Electric Power Plants. The applications to be studied are:

1. Condensate boost pump for a turboelectric plant using potassium. Design Point: 1.5 pps, 1200°F., 100 ft. developed head.

2. Primary coolant pump for a turboelectric or thermionic plant using lithium. Design Point: 40 pps, 1700°F., 6 psi pressure rise.

3. Radiator coolant circulating pump for either turboelectric or thermionic:
   (a) using lithium. Design Point: 2 pps, 1200°F., 20 psi pressure rise.
   (b) using NaK. Design Point: 6 pps, 1200°F., 25 psi pressure rise.

The program consists of three phases. Phase I is research only. Phase II is construction and demonstration of selected pumps. Phase III is final evaluation.

The objectives of Phase I of the program are to determine the feasibility of using EM pumps in Space Electric Power Plants, establish the bases for selecting pumps for specific application, establish the bases for design of EM

pumps applicable to space power plants, select pumps for construction and test and establish a test program for the selected pumps.

This report covers the period from December 27, 1963 to February 27, 1964. The principle events of the reporting period were:

1. The following additions to the Design Data Book:
   a) A design chart for stored energy in magnetic circuit air gaps.
   b) Analytical methods for D.C. conduction pumps.
   c) Analytical methods for the single phase induction pump.
   d) Physical properties of a number of columbium molybdenum and tantulum alloys for pump duct application.
   e) The dielectric properties of several gases for heat transfer use in induction pump stator cavities.
   f) A preliminary design for a boiler feed pump, together with several other pumps reported in the last Quarterly.

2. The computor program for single phase induction pumps was proved out.

II. DISCUSSION

In studying the effect of power factor on weight of pump systems the low power factor characteristic of induction pumps was investigated. Some generalized relationships were developed whereby the power factor for a given design may be determined. The derivations and analytical procedure along with two sets of curves were added to Section II-A of the DDB. Appendix I shows the addition.

The analysis of D.C. pumps and methods for prediction of performance was completed. The entire Section II-B-2 as added to the DDB is shown in Appendix I. The analysis covers both permanent and electromagnet excited pumps. A five step procedure is presented:

1. Calculation of internal pressure drop.
2. Determination of total pressure rise required.
3. Calculation of magnetic field.
4. Calculation of current, voltage, power and efficiency.
5. Corrections for "armature reaction" effects.

The work on single phase induction pumps was completed. This has been issued as Section II-B-3 in the DDB. Appendix I shows this addition.

It is interesting to note that the single phase induction pump has received little attention in the past. AERE #1090, by Watt, is the only reference available in which a quantitative analysis of this pump type is attempted. This analysis is partly graphical and is not in suitable form for application to a variety of pump designs. The initial appraisal of the single phase induction pump was that, because it does not have a well defined "synchronous speed", it

might have unique adaptability to high frequency power. Accordingly, an analysis of the performance of two single phase EM pump configurations was carried out. The configuration treated by Watt has been modified to improve symmetry and reduce size and weight. Calculations indicate that this pump type is best suited to high flow, low pressure applications, such as the primary coolant pump application in the thermionic power system. Preliminary indications are that attractive efficiency and weight are possible in the primary coolant pump application provided a satisfactory duct inlet and exit arrangement can be developed. Layouts of these regions will be made shortly. Calculations have also shown that a low frequency power supply is essential to good pump efficiency. Output pressure is pulsating as in all single phase EM pumps. The extent to which the single phase induction EM pump will be studied during the remainder of the Contract depends upon the development of suitable duct inlet and outlet connections and upon the problems associated with the introduction of single phase loads of this magnitude into the power system.

Physical properties data obtained for several refractory metals and alloys were introduced into the Design Data Book, Section III-B "Duct Materials". Molybdenum and molybdenum alloys properties presented include tensile strength, hardness, elongation and stress-rupture together with the effects of processing variables on all of these properties. Unalloyed molybdenum and seven alloys are covered, the most important being Mo-$\frac{1}{2}$ Ti, TZM and TZC.

Columbium and its principle alloys, AS-55, AS-30, F-48 and D-43, are all represented. In some cases only tensile strength is presented but for Cb and Cb-1Zr the data are adequate for preliminary design purposes.

Several tantalum alloys are included in the data -- notably, T-111 which is interesting as a duct material because its ratio of resistivity to stress-rupture strength is more favorable than Cb-1Zr. In general, however, the less common physical properties such as resistivity are frequently not available on the exotic materials.

The volume of this addition to the DDB is such that it is impractical to reproduce it all here. Appendix II presents a sampling of the data discussed above.

The induction pump thermal design presented in the Second Quarterly Report whereby the stator would be cooled by enclosing it in a gas filled envelope introduced the need for gas properties data. Helium was recognized as the outstanding choice from the heat transfer views; however, its dielectric strength was doubtful. Information on dielectric strength of various gases was obtained and on this information the preliminary choice of nitrogen, as mentioned below, was based. The gas data was added to the DDB as shown in Appendix II.

The condensate boost pump and radiator coolant pump as described in Quarterly Progress Report No. 2 were added to Section VII of the DDB. In the course of performing the analytical work for the condensate boost application it became evident that a helical induction pump could easily do the full boiler feed job without need of a booster.

Although the boiler feed pump is not specifically designated as a required application, it appeared sufficiently attractive to warrant preliminary calculations. The resultant preliminary design is illustrated on the following page as Figure 1. The complete addition to the DDB is given in Appendix III including the radiator

coolant and condensate boost pumps.

As a matter of interest some information on canned motor pumps for boiler feed application was obtained by phone conversation with the AEC-SNAP 50 Office. The information on the EM pump vs. the canned motor pump is summarized below. The canned motor unit requires a jet booster on the suction side which is included in the weight.

BOILER FEED PUMPS

TURBOELECTRIC SPACE POWER PLANT

	EM Pump	Canned Motor Pump
Flow	1.5 lb/sec	2 lb/sec
Head	100 psi	100 psi
Power	10 KVA	9 KVA
Weight	105 lb.	145 lb.

As reported previously the single phase induction pump had several attractive features. In order to permit rapid evaluation of single phase designs and assist in making good choices the analytical method shown in Appendix I was programmed for the IBM 650 computor. Some difficulty was initially experienced in validating the program over the full range of interest. Hand calculations are commonly used for this purpose. The problem was corrected during the past month and the program is now proven reliable. Several pump models for radiator coolant and primary coolant applications are being investigated. The single phase pump is best suited to low head applications.

III. PROJECTION

During the coming month several single phase pump designs will be run to evaluate the applicability of this type of pump to space power plants.

Several D.C. pump designs will be run to more fully evaluate this pump type. The thermionic power plant applications will be stressed.

Properties data for magnetic materials and for some ferrous duct alloys will be added to the design data book. Additional information on gases will be obtained.

Weight penalty values will be determined for pump cooling and for low power factor.

Reliability review of selected designs will be initiated. Basic reliability considerations will be established.

APPENDIX I

DESIGN DATA BOOK ADDITION

SECTION II

EM PUMP DESIGN CONSIDERATION

Analysis of Performance

An analysis by D. A. Watt of a single phase induction pump with an annular duct was published in Reference 1 in 1953. Reference 2, a declassified edition of Reference 1, was published in 1956. The configuration treated in these references is shown in Figure 1.

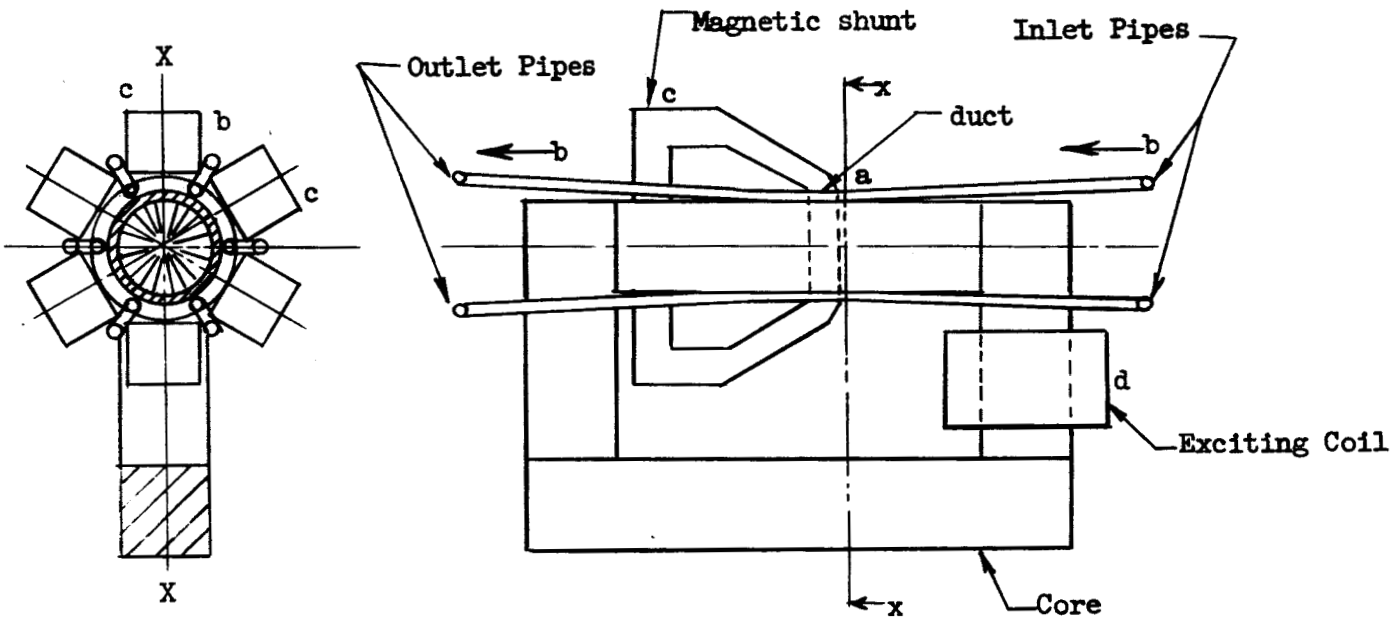

Figure 1

SINGLE PHASE INDUCTION PUMP STUDIED BY WATT

A more compact configuration developed during the course of this EM pump design study is shown in Figure 2.

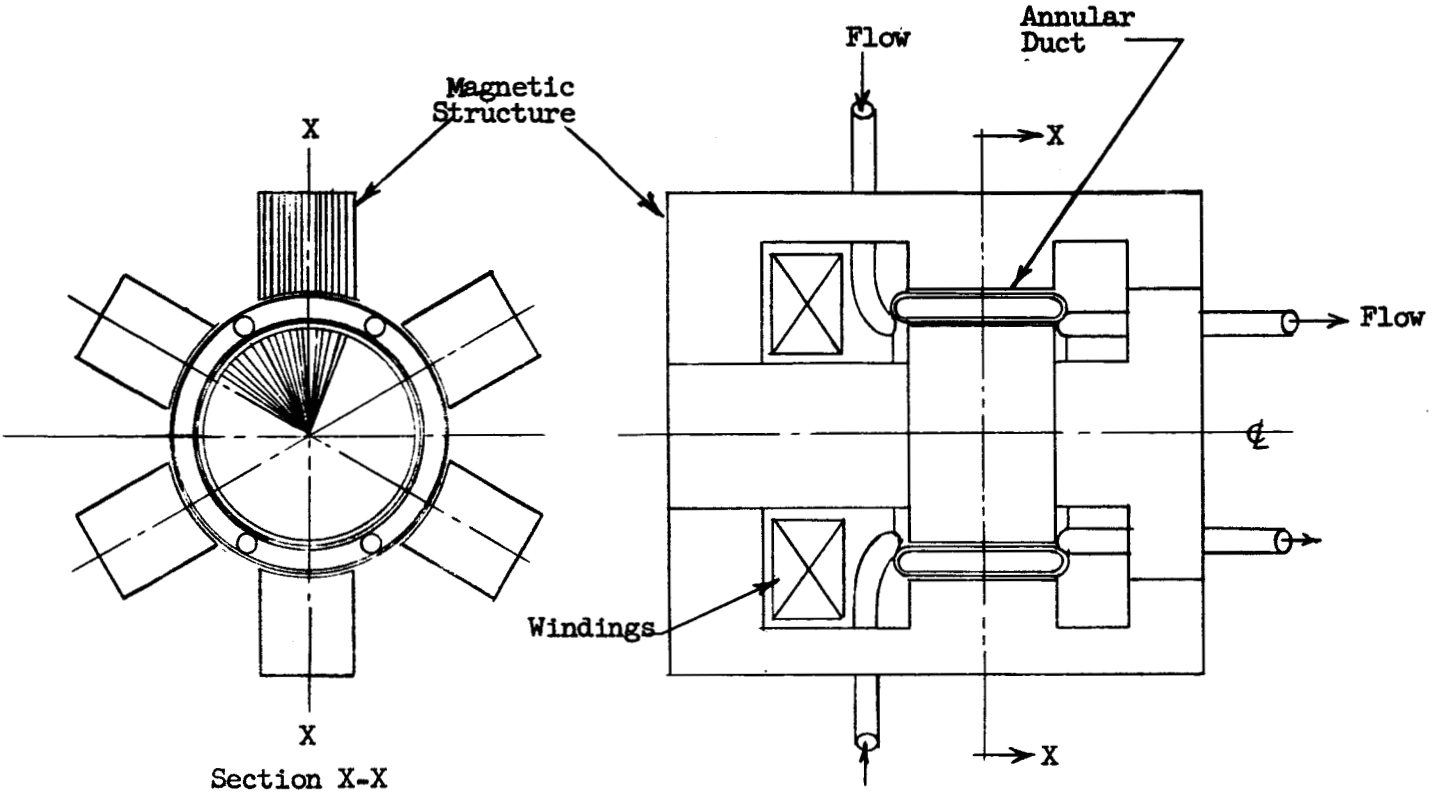

Figure 2

SINGLE PHASE INDUCTION PUMP, TYPE A

From an electromagnetic viewpoint this configuration is equivalent to that studied by Watt. It is more compact and more symmetrical, hence better suited to space applications where size, weight, and volt ampere requirements must be minimized. As illustrated in Figure 2, both the duct and the exciting coil are annular in form. The basic magnetic flux pattern is axial and radial,

hence the laminations must be oriented with their major dimensions lying in planes passing through (or near) the axial centerline of the pump. Multiple inlet and outlet pipes are desirable to minimize hydraulic and electromagnetic inlet and exit losses. The symmetry of the configuration of Figure 2 is such that the complex arrangement of chokes described by Watt in the reference to minimize circulating currents in the configuration of Figure 1 are not necessary provided entry and exit pipes are arranged with appropriate symmetry.

Other compact single phase induction pump configurations similar to that of Figure 2 are shown in Figures 3 and 4.

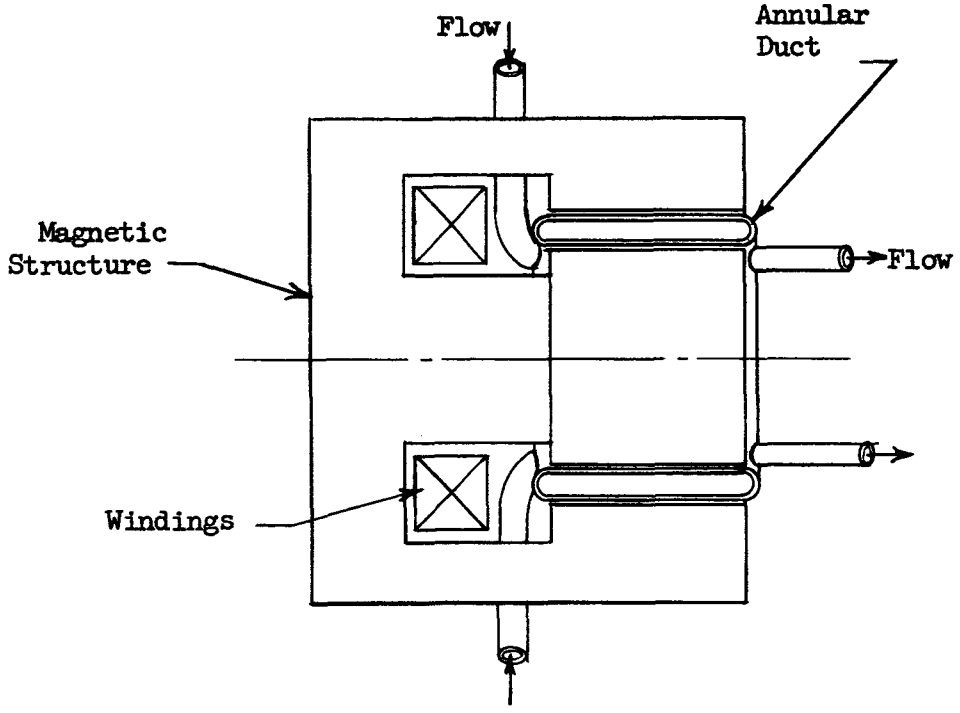

Figure 3

SINGLE PHASE INDUCTION PUMP, TYPE B

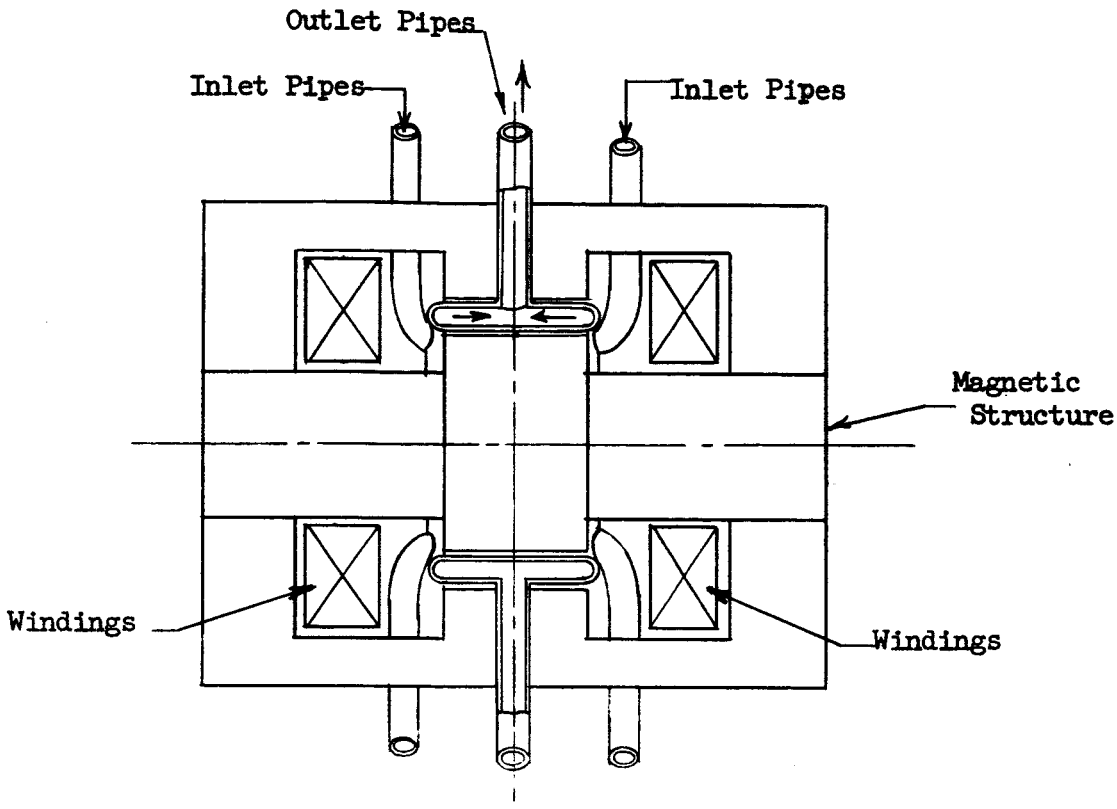

Figure 4

SINGLE PHASE INDUCTION PUMP, TYPE C

The configuration of Figure 3, Type B, is somewhat more compact than Type A, but this compactness is achieved at the expense of poorer performance. Type C, shown in Figure 4, has exciting coils located at each end of the annular duct. When these coils are connected with their mmf's aiding, considering axial flux, Type C may be shown to be equivalent to two pumps of Type A, connected back to back. Similarly, when the coils are connected with their mmf's opposing, Type C may be shown to be equivalent to two pumps of Type B, connected back to back. In either case, pumping is from the ends of the duct toward the middle. Type C does not appear to have any significant advantages relative to Types A and B.

The analysis of the performance of single phase induction pumps Types A and B proceeds along similar lines and is carried through concurrently below.

Throughout this analysis the following assumptions are made:

1. The annular duct and air gap configuration is treated as an equivalent rectangular configuration as shown in Figure 5. This introduces negligible error as the duct diameter will normally be several intergral multiples of the air gap radial height.

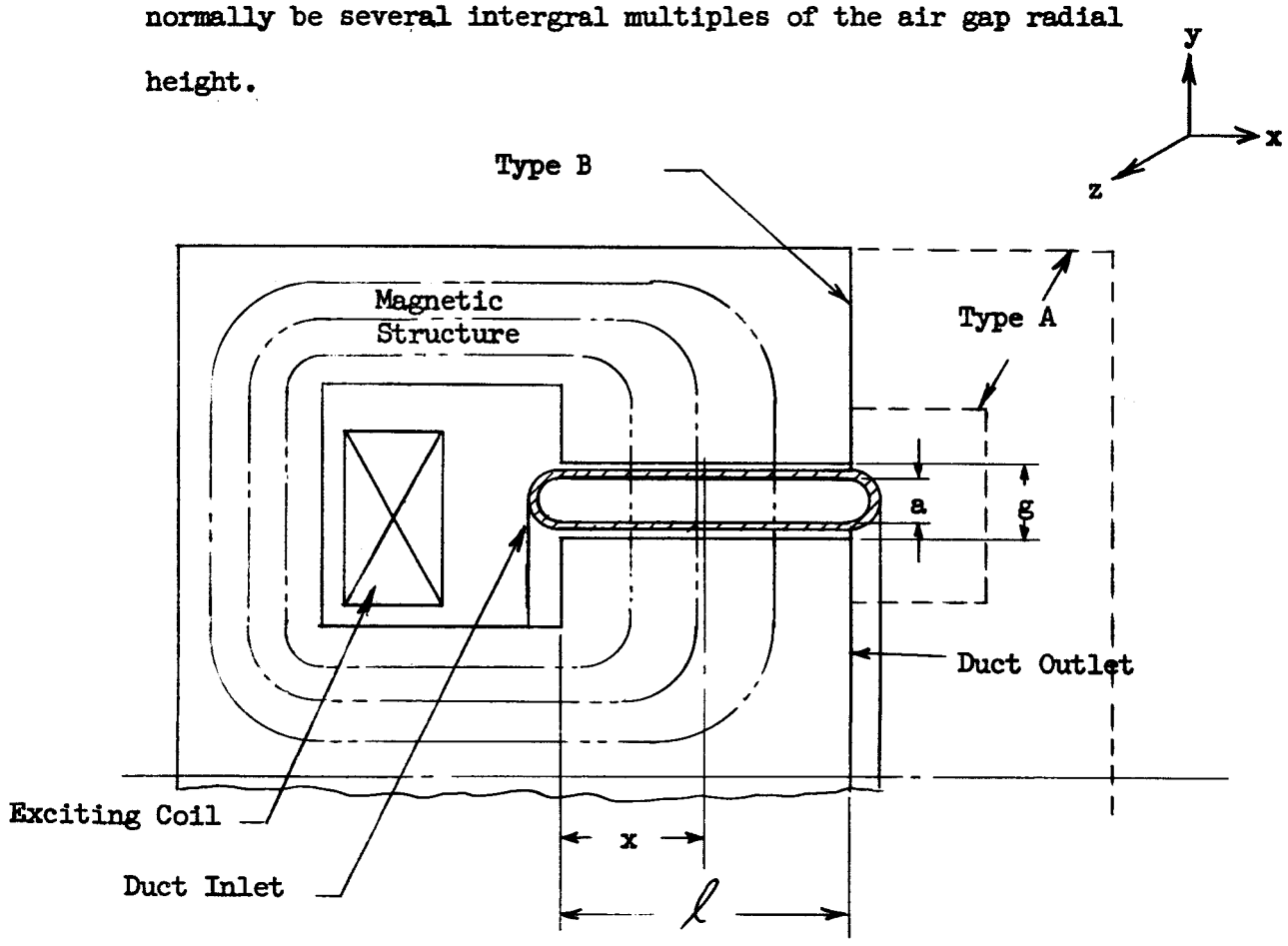

FIGURE 5

EQUIVALENT CONFIGURATION FOR ANNULAR DUCT DESIGN

2. The flux density in the air gap is assumed to have a y-component only.
3. The fringing flux field at each end of the duct is neglected.
4. The permeability of the magnetic core is assumed infinite during the analysis of the air gap region. A correction for mmf drop in

the core may be made later.

5. Fluid and duct walls are assumed to be isotropic and non-magnetic, having permeabilities the same as free space.

6. The fluid velocity is assumed to have an x-component only and to be independent of y and z.

The following nomenclature is used. All sinusoidally varying quantities are rms. Any consistent system of units applies to the analysis. The results are expressed in terms of the units indicated.

B = Flux density in duct, y-axis, kilolines/in^2

ϕ = Flux in core at any point x, measured from duct inlet, megalines

μ = Permeability of air gap, 3.19 $\frac{\text{lines}}{\text{amp in}}$

j_f, j_d = Current density in fluid and duct walls, respectively, z-axis, $\frac{\text{amperes}}{\text{in}^2}$

ρ_f, ρ_d = Electrical resistivity of fluid and duct walls, respectively, $\mu\Omega$-in.

d = Mean duct diameter, inches

a = Height (radial) of fluid in duct, inches

t = Duct wall thickness, inches

g = Total non-magnetic air gap, inches

P = Developed pressure, psi

Q = Flow, gpm

v = Fluid velocity, ft/sec

f = Frequency of power supply, cps

w = $2\pi f$, ft/sec

M = Magmetomotive force across air gap, amperes

V_t = Volts per turn in exciting coil, volts

R_o = Resistance of duct inlet header, ohms

R_ℓ = Resistance of duct outlet header, ohms

R_c = Resistance of coil, assuming one turn, ohms

W = Power, watts

VAR = Reactive power

η = Efficiency

P.F. = Power factor

D_1, ϕ_1, ϕ_2, X_1 = Constants, defined when introduced

$\alpha_1, \alpha_2, \gamma_1, \gamma_2, \beta_1, \beta_2$ = Constants, defined when introduced

The following basic relationships may be written by inspection of Figure 5.

$$B = -\frac{1}{\pi d} \frac{\partial \phi}{\partial x} \tag{1}$$

$$j_f = -\frac{1}{\pi d \rho_f} \left(\frac{\partial \phi}{\partial t} + v \frac{\partial \phi}{\partial x}\right) \tag{2}$$

$$j_d = -\frac{1}{\pi d \rho_d} \frac{\partial \phi}{\partial t} \tag{3}$$

$$\frac{\partial B}{\partial x} = \frac{\mu}{g} (A j_f + 2t j_d) \tag{4}$$

For an assumed configuration and fluid velocity, these equations relate the four unknowns, B, ϕ, j_f, and j_d. They may be combined to yield one equation in one unknown, ϕ

$$\frac{\partial^2 \phi}{\partial x^2} = \frac{\mu_e}{\rho_f g} \left\{ \left(1 + \frac{2t}{a} \frac{\rho_f}{\rho_g}\right) \frac{\partial \phi}{\partial t} + v \frac{\partial \phi}{\partial x} \right. \tag{5}$$

Assuming the exciting voltage to be sinusoidal in time and the fluid velocity to be constant, the system is linear and the resulting flux ϕ will also be sinusoidal in time. Thus, we may write

$$\phi = R_e \left\{ \Phi \varepsilon^{iwt} \right\} \tag{6}$$

and $$\frac{\partial \phi}{\partial t} = R_e \left\{ iw \Phi \varepsilon^{iwt} \right\} \tag{7}$$

where $R_e \left\{ A \right\}$ signifies "the real part" of A.

For convenience, let

$$D_1 = \left[1 + \frac{2t}{a} \quad \frac{\rho_f}{\rho_d} \right] \tag{8}$$

Then, substituting these relationships in Equation (5), and dropping the $R_e \left\{ \quad \right\}$ designation for convenience, in the conventional manner, Equation (5) may be written

$$\frac{\partial^2 \Phi}{\partial x^2} - \frac{\mu_{av}}{\rho_f g} \quad \frac{\partial \Phi}{\partial x} - j \frac{W \mu D_1 a}{\rho_f g} \Phi = 0 \tag{9}$$

The solution of this equation is

$$\Phi = \Phi_1 \varepsilon^{\partial_1 x} + \Phi_2 \varepsilon^{\partial_2 x} \tag{10}$$

Where

$$\partial_1 = \partial_1 + i\beta_1 = \frac{\mu_{av}}{2 \rho_f g} \left\{ 1 - \sqrt{1 + i \frac{4w \rho_f g D_1}{\mu_{av^2}}} \right\} \tag{11}$$

$$\partial_2 = \partial_2 + i\beta_2 = \frac{\mu_{av}}{2 \rho_f g} \left\{ 1 + \sqrt{1 + i \frac{4w \rho_f g D_1}{\mu_{av^2}}} \right. \tag{12}$$

It is apparent that $$\beta_1 = -\beta_2$$

Φ_1, and Φ_2 are constants which depend upon the boundary conditions. It is convenient to proceed with the analysis of the pump performance, expressing the performance in terms of these constants. Their evaluation in terms of the boundary conditions for pumps Type A and B will be covered later.

It is convenient to introduce a dimensionless constant C_1, where

$$C_1 = \frac{\Phi_2}{\Phi_1} \tag{13}$$

Equation (10) may then be written

$$\Phi = \Phi_1 \left\{ \varepsilon^{\partial_1 x} + C_1 \varepsilon^{\partial_2 x} \right\} \tag{14}$$

Substituting now from Equation (14) in Equation (1), (2) and (3), we may write

$$B = - \frac{\Phi_1 \partial_1}{\pi d} \left[\varepsilon^{\partial_1 x} + \frac{\partial_2}{\partial_1} C_1 \varepsilon^{\partial_2 x} \right] \tag{15}$$

$$j_f = - \frac{\Phi_1 w}{\pi d\, f_d} \left\{ \left(\frac{v}{w} \partial_1 + i \right) \varepsilon^{\partial_1 x} + \left(\frac{v}{w} \partial_2 + i \right) C_1^{\partial_2 x} \right\} \tag{16}$$

$$j_d = - \frac{\Phi w}{\pi d\, f_d} \left\{ \varepsilon^{\partial_1 x} + C_1 \varepsilon^{\partial_2 x} \right\} \tag{17}$$

The pressure developed by the pump is given by the product of the flux density and the current density in the fluid, integrated over the length of the pump duct. This pressure varies sinusoidally in time. The average value of the pressure is given by the expression

$$p = R_e \left\{ \int_0^{\ell} -j_f \bar{B}\, dx \right\} \tag{18}$$

where $\bar{B}$ is the complex conjugate of B

Thus

$$p = R_e \left\{ - \frac{w \Phi_1 \bar{I}_1 \bar{\partial}_1}{(\pi d)^2 \rho_f} \int_0^{\ell} \left[\left(\frac{v}{w} \partial_1 + i \right) \varepsilon^{\partial_1 x} + \left(\frac{v}{w} \partial_2 + i \right) C_1 \varepsilon^{\partial_2 x} \right] \left[\varepsilon^{\bar{\partial}_1 x} + \bar{C}_1 \left(\frac{\bar{\partial}_2}{\bar{\partial}_1} \right) \varepsilon^{\bar{\partial}_2 x} \right] dx \right\} \tag{19}$$

The expression of Equation (19) may be expanded, integrated and expressed as follows:

$$p = - \frac{w}{\rho_f} \left[\frac{|\Phi_1|}{\pi d} \right]^2 R_e \left\{ \left(\frac{v}{w} \partial_1 + i \right) \left[\frac{\bar{\partial}_1 (\varepsilon^{2 \partial_1 \ell} - 1)}{2 \partial_1} + \bar{\partial}_2 \bar{C}_2 \right] + \left(\frac{v}{w} \partial_2 + i \right) \left[|C_1|^2 \frac{\bar{\partial}_2 (\varepsilon^{2 \partial_2 \ell} - 1)}{2 \partial_2} + \bar{\partial}_1 X_3 \right] \right\} \tag{20}$$

where
$$C_2 = C_1 \left[\frac{\varepsilon^{(\bar{\partial}_1 + \partial_2)\ell_{-1}}}{\bar{\partial}_1 + \partial_2} \right] \tag{21}$$

and $|A|$ means "the absolute value of A".

It is apparent from Figure (5) that the total flux entering the duct is the value of the flux at X = 0 and the total mmf produced by the exciting coil, neglecting iron drop, may be written in terms of the air gap flux density at X = 0 and the mmf produced by the inlet duct header. Thus

$$\bar{\Phi}_T = \bar{\Phi}_1 \left\{ 1 + C_1 \right\} \tag{22}$$

$$M_c = \frac{g}{\mu} B\Big/_{x=o} + \frac{iw\bar{\Phi}_T}{R_o} \tag{23}$$

Thus, from Equation (15)

$$M_c = -\frac{w\bar{\Phi}_1}{R_o}\left(\frac{gR_o}{w\mu\pi d}\partial_1 - i\right) + \left(\frac{gR_o}{w\mu\pi d}\partial_2 - i\right) C_1 \Bigg\} \tag{24}$$

Assuming a single turn exciting coil, the component of applied voltage corresponding to the flux ϕ_T is

$$V_1 = \frac{\partial\bar{\Phi}t}{\partial t} = jw\bar{\Phi}_1 \left[1 + C_1 \right] \tag{25}$$

The total input power to the air gap region is

$$W_m = R_e \left\{ M_c \bar{V}_1 \right\} \tag{26}$$

or, using Equation (24) and (25)

$$W_m = \frac{w^2 \bar{\Phi}_1 \bar{\Phi}_1}{R_o} Re \left\{ i (1 + C_1)\left[\frac{g R_o}{w\mu\pi d} \partial_1 - i + \left(\frac{g R_o}{w\mu\pi d}\partial_2 - i\right) C_1 \right] \right\} \tag{27}$$

Also

$$VAR_m = \frac{w^2 \Phi_1 \bar{\Phi}_1}{R_o} \mathrm{Im}\left\{ i\,(1+\bar{C}_1)\left[\left(\frac{g\,R_o}{w\mu\pi d}\partial_1 - i\right) + \left(\frac{g\,R_o}{w\mu\pi d}\partial_2 - i\right) C_1 \right] \right\} \quad (28)$$

If the exciting coil resistance, on a one turn basis is R_e, the coil loss may be written

$$W_c = |M_c|^2 R_c \quad (29)$$

The total loss is the sum of W_m and W_c

$$W_T = W_m + W_c \quad (30)$$

The power output is given by the product of developed pressure and flow. Thus, in consistent units, efficiency and power factor may be written

$$\eta = \frac{pQ}{W_T} \quad (31)$$

$$P.F. = \frac{W_T}{\sqrt{\overline{VAR_m}^2 \quad \overline{W_T}^2}} \quad (32)$$

The turn voltage is

$$V_t = \frac{\sqrt{\overline{VAR_m}^2 \quad \overline{W_T}^2}}{M_c} \quad (33)$$

The analysis is now complete except for further consideration of the constants, Φ_1 and C_1, which are defined by Equation (14), repeated for convenience.

$$\Phi = \Phi \left\{ \varepsilon^{\partial_1 x} + C_1 \varepsilon^{\partial_2 x} \right\} \quad (14)$$

One boundary condition common to both pumping configurations Type A and Type B is that the total flux entering the duct, Φ_T, is the value of Φ at $X = 0$. This

condition has been expressed in Equation (22)

$$\Phi_T = \Phi_1 (1+C_1) \tag{22}$$

A second boundary condition is imposed at the outlet end of the duct, at $X = \ell$.

For pump Type A, the mmf drops around a closed path crossing the duct at $X = \ell$ and returning to the starting point by way of the magnetic core to the right of the duct (Figure 5) yield this relationship.

$$I_\ell = -\frac{g B}{\mu}\Big/_{x=\ell} = \frac{g \partial_1}{\mu \pi d} \Phi_1 \left[\varepsilon^{\partial_1 \ell} \frac{\partial_2}{\partial_1} C_1 \varepsilon^{\partial_2 \ell}\right] \tag{34}$$

where I_ℓ is the current in the outlet duct header, having resistance R_ℓ. I_ℓ flows by virtue of the voltage induced by the flux at $X = \ell$. Thus,

$$I_\ell = -\frac{iw\Phi}{R_\ell}\Big/_{x=\ell} = -\frac{iw\Phi_1}{R_\ell}\left[\varepsilon^{\partial_1 \ell} + C_1 \varepsilon^{\partial_2 \ell}\right] \tag{35}$$

Combining Equations (23) and (24), and solving for C_1,

For Type A,

$$C_1 = -\frac{\left(\frac{g R}{w \mu \pi d} \partial_1 + i\right)}{\left(\frac{g R}{w \mu \pi d} \partial_2 + i\right)} \varepsilon^{(\partial_1 - \partial_2)\ell} \tag{36}$$

For pump Type B, the boundary condition at $X = \ell$ is more obvious. Neglecting fringing flux, the flux at $X = \ell$ must be zero. Thus for Type B, from Equation (14) at $X = \ell$,

$$C_1 = -\varepsilon^{(\partial_1 - \partial_2)\ell} \tag{37}$$

Summary of Performance Equations

The equations relating the performance of a single-phase induction pump of either Type A or Type B to the parameters of the configuration and the fluid pumped are extracted from the foregoing analysis and listed below. The equations in the analysis are correct in any consistent system of units. Constants have been introduced into the equations listed below to correspond to the units indicated in the Nomenclature. These equations have the same numbers as the corresponding equations in the analysis, except that a lower case "a" has been added as a suffix.

$$D_1 = \left[1 + \frac{2t}{a}\,\frac{\rho_f}{\rho_d}\right] \qquad \text{dimensionless} \qquad (8a)$$

$$D_2 = \sqrt{1 + i\ 5.475\ \frac{f \rho_f g D_1}{a v^2}}$$

$$\partial_1 = \partial_1 + i\beta_1$$

$$\partial_2 = \partial_2 + i\beta_2$$

$$\partial_1 = 0.1915\ \frac{av}{\rho_f g}\ \left[1 + \mathrm{Re}\,(D_2)\right]$$

$$\partial_2 = 0.1915\ \frac{av}{\rho_f g}\ \left[1 + \mathrm{Re}\,(D_2)\right]$$

$$\beta_1 = -\beta_2 = 0.1915\ \frac{av}{\rho_f g}\ \mathrm{Im}\,(D_2)$$

(11a), (12a)

For pump Type A,

$$C_1 = -\left[\frac{1.588 \times 10^6 \left(\frac{g\,R_\ell}{f_d}\right)\partial_1 + i}{1.588 \times 10^6 \left(\frac{g\,R_\ell}{f_d}\right)\partial_2 + i}\right] \varepsilon^{(\partial_1 - \partial_2)\ell}, \quad \text{dimensionless}$$

For pump Type B

$$C_1 = -\varepsilon^{(\partial_1 - \partial_2)\ell} \quad \text{, dimensionless}$$

$$C_2 = C_1\left[\frac{\varepsilon^{(\bar{\partial}_1 + \partial_2)\ell} - 1}{\bar{\partial}_1 + \partial_2}\right] \quad \text{, inches} \qquad (21a)$$

$$\Phi_T = \Phi_1\left\{1 + C_1\right\} \quad \text{, megalines} \qquad (22a)$$

$$G = \left[1.588 \times 10^6 \left(\frac{gR_o\partial_1}{f\,d}\right) - i\right] + \left[1.588 \times 10^6 \left(\frac{gR_o\partial_2}{f\,d}\right) - i\right] C_1, \text{ dimensionless}$$

$$M_c = -0.0628 \frac{f\Phi_1}{R_o} G \quad \text{, amperes} \qquad (24a)$$

$$KW_m = 3.95 \times 10^{-6} \frac{[f|\Phi_1|]^2}{R_o} \mathrm{Re}\left\{i\,(1 + C_1)\,G\right\} \quad \text{kilowatts} \qquad (27a)$$

$$KVAR_m = 3.95 \times 10^{-6} \frac{[f|\Phi_1|]^2}{R_o} \mathrm{Im}\left\{i\,(1 + C_1)\,G\right\} \quad \text{kilovars} \qquad (28a)$$

$$KW_c = 10^{-3} \left|M_c\right|^2 R_c \quad \text{kilowatts} \qquad (29a)$$

$$KW_T = KW_m + KW_c \quad \text{kilowatts} \qquad (30a)$$

$$V_t = 10^3 \frac{\sqrt{(KW_T)^2 + (KVAR_m)^2}}{M_c} \quad \text{volts} \qquad (33a)$$

$$P.F. = \frac{KW_T}{\sqrt{(KW_T)^2 + (KVAR_m)^2}} \quad \text{dimensionless} \qquad (32a)$$

$$\text{Efficiency} = \eta = \frac{0.435\,p\,Q}{10^3\,KW_T} \quad \text{dimensionless} \qquad (31a)$$

It follows from Equations (14) and (15) that the flux at $x = \ell$, Φ_ℓ, and gap flux density at $x = o$ and $x = \ell$, B_o and B_ℓ, respectively, are

$$\Phi_\ell = \Phi_1 \, \varepsilon^{\partial_2 \ell} \left\{ \varepsilon^{(\partial_1 - \partial_2)\ell} + C_1 \right. \quad \text{megalines} \tag{14a}$$

$$\left.\begin{aligned} B_o &= -10^3 \, \frac{\Phi_1 \partial_1}{\pi d} \left\{ 1 + \frac{\partial_2}{\partial_1} C_1 \right\} \quad \text{kilolines/in}^2 \\ B_\ell &= -10^3 \, \frac{\Phi_1 \varepsilon^{\partial_2 \ell} \partial_1}{\pi d} \left\{ \varepsilon^{(\partial_1 - \partial_2)\ell} + \frac{\partial_2}{\partial_1} C_1 \right. \quad \text{kilolines/in}^2 \end{aligned}\right\} \tag{15a}$$

II. EM Pump Design Considerations

B. Performance Prediction

2. D-C Conduction Pumps

The d-c conduction electromagnetic pumps considered in the following section are of the type shown in the sketch of Figure II-101

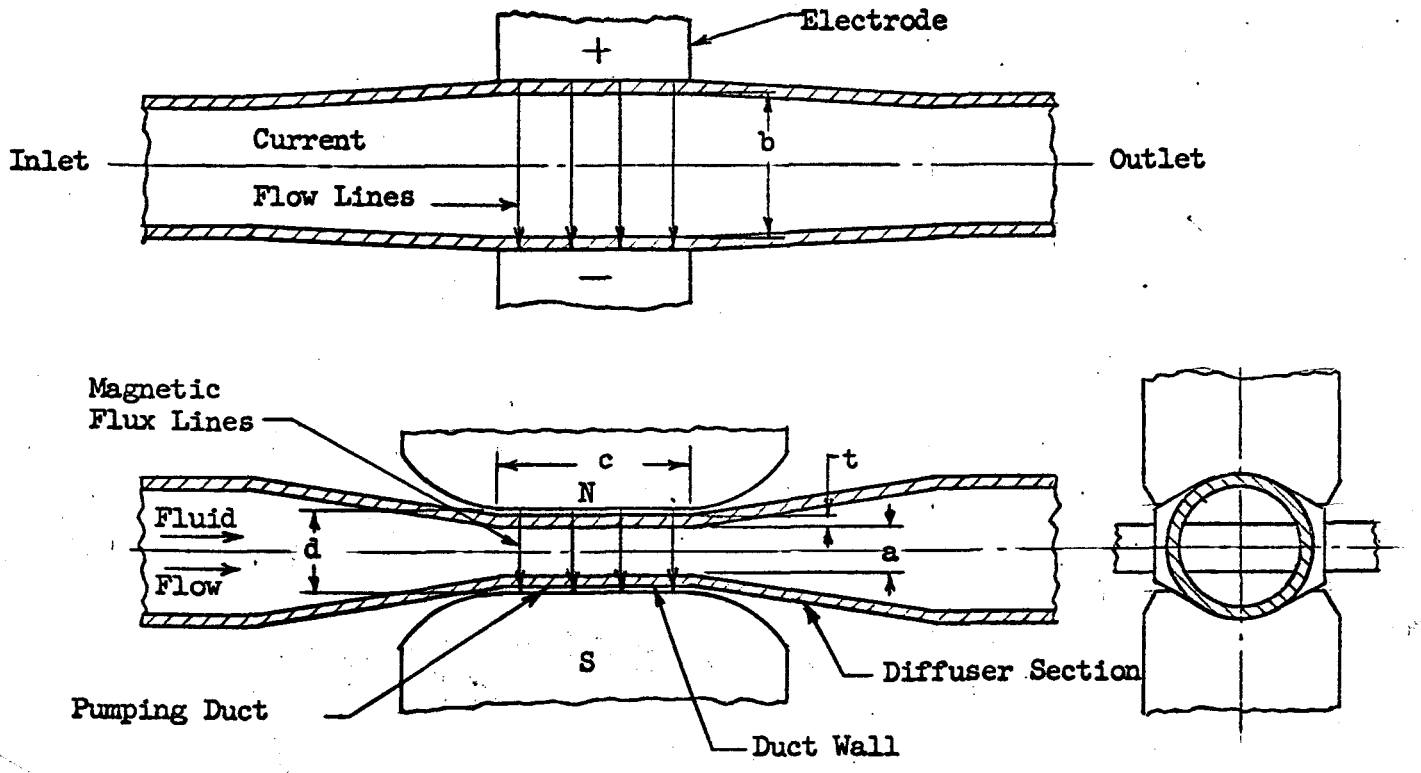

Figure II-101
D-C CONDUCTION PUMP

The fluid enters the pump by way of an inlet diffuser section leading to a pumping section of rectangular cross section and constricted area. Here the interaction between the current and the magnetic field produces an increase in fluid pressure, and the fluid flows on through the outlet diffuser to the pump outlet.

The magnetic field and current relationships are shown in the sketch. The magnetic field may be provided by a permanent magnet, particularly in small-size pumps, or by an electromagnet. If an electromagnet is used its exciting winding is usually connected in series with the current electrodes.

If the duct is made of conducting material, current is introduced into the fluid by electrodes attached to the outside of the duct walls. If the duct is of non-conducting material the electrodes extend through the walls and make contact directly with the fluid.

The equivalent electrical circuit for this pump is shown in Figure II-102.

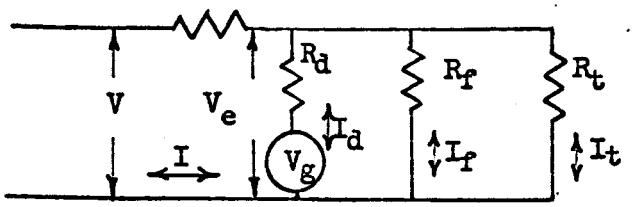

Figure II-102

D-C CONDUCTION PUMP EQUIVALENT CIRCUIT

The resistance R_d represents the resistance of the fluid directly between the electrodes. The current, I_d, through this portion of the fluid reacts with the magnetic field to produce the increase in pressure in the fluid. The flow of fluid through the magnetic field generates a back emf, V_g, which opposes the flow of current I_d. The resistance R_f represents the resistance of the two parallel fringing current paths from the ends of the electrodes through the fluid out into the diffuser sections around the magnetic field region. Current in these paths, I_f, does not contribute to the development of pressure in the fluid except as the fringing magnetic field may extend into that region. R_t represents the resistance of the current path through the duct walls from electrode to electrode. The current in this path, I_t, does not contribute to the development of pressure in the fluid. The resistance R_e represents the resistance of the electrodes

through which the entire current passes. It includes the resistance of the joint between the electrode and the duct wall and a part of the resistance through the thickness of the duct wall. Part of the resistance through the thickness of the duct wall and contact resistance between the duct wall and the fluid may be included in R_d and R_f. If the duct is made of non-conducting material there is no duct wall current, and the electrodes contact the fluid directly. If the magnetic field is produced by a series electromagnet, R_e includes the resistance of the magnet coil.

The magnet poles may be tapered back from the pumping portion of the duct to extend the fringing magnetic field into the region of fringing current . Figure II-101. This tends to reduce the fringing current and t... ging field contributes to the pressure rise by reacting with the fr ging current. Non-conducting separators (not shown) may be located in the diffuser sections to block much of the fringing current.

The calculation of voltage, current and power required to produce a desired flow and pressure rise in a pump of known construction and dimensions involves the following steps:

1) Calculation of internal pressure drop.

2) Calculation of total pressure rise necessary.

3) Calculation of magnetic field.

4) Calculation of current, voltage, power and efficiency.

5) Corrections for "armature reaction" effects.

These steps will be discussed and methods of calculation described.

1) Calculation of Internal Pressure Drop.

There is a pressure drop in the pump, due to hydraulic losses in the duct and diffuser sections, which must be added to the net pressure rise developed by the pump in order to obtain the total pressure rise to be generated in the duct by the current and magnetic field.

The loss in the duct portion of the pump where the pumping takes place may be calculated as follows:

$$P_d = C_f c \frac{2\sigma v^2}{g d_d \times 144} \quad (1)$$

$$d_d = 2a\,b/(a+b) \quad (2)$$

P_d = pressure drop, psi, in the duct

C_f = friction factor - dimensionless

σ = fluid density - lb/cu. ft.,

d_d = hydraulic diameter of duct-inches

c = length of duct - inches

v = velocity of fluid in the duct - ft/sec

g = 32.2 ft/sec^2.

a = height of duct - inches

b = width of duct - inches

The value of C_f may be materially affected by the presence of the magnetic field crossing the duct. The effect is to increase the hydraulic loss when the flow is laminar and to increase the value of the Reynolds number at which transition from laminar to turbulent flow occurs. The magnetic field is not thought to affect the hydraulic loss significantly after turbulent flow is established.

The relationships between friction factor, Reynolds number and Hartmann are developed and illustrated in Section II-A "General Relationships".

Calculation of pressure drop in the duct by means of these relationships does not take into account losses occurring at the ends of the duct. These may be a significant proportion of the total in d-c conduction pumps because the ducts are usually only a few diameters long. They depend upon the shape of the diffuser sections connecting to the duct, and may be conveniently included as part of the losses in these sections.

Pressure drop in the diffuser sections can be calculated for conical, square, or rectangular shapes. The accuracy of results for a circular-to-rectangular shape, in the presence of the fringing magnetic field, may be poor. The drop may be estimated by assuming an arbitrary number of velocity heads loss.

$$P_{dif} = \frac{K\sigma v^2}{144 \times 2g}$$

(8) P_{dif} = pressure drop in diffuser sections, psi

σ = fluid density - lb/cu. ft.

v = velocity of fluid in the pumping duct, ft/sec.

K = number of velocity heads assumed

g = 32.2 ft/sec.^{2}

The value of K may be estimated by comparing the pump with a Venturi meter. For Venturi meters with diameter ratios of 25 to 50% an entrance cone of 21 deg. and an exit cone of 5 to 7 deg. the overall pressure loss is given[1] as 10 to 20% of the differential pressure.

$$P = \frac{\sigma}{144}\left[\frac{v^2 - v_o^2}{2g}\right] = \frac{\sigma}{144}\left[1 - \left(\frac{A}{A_1}\right)^2\right]\frac{v^2}{2g}$$

$$P_{loss} = 0.2\left[1 - .0625\right]\ \frac{\sigma}{144}\ \frac{v^2}{2g}\ , \left(\frac{A}{A_1} = \frac{1}{4}\right)$$

$$K = 0.2(1-.0625) = 0.187$$

(9) A = area of pumping duct - sq. in.

A_1 = area of inlet and exit pipes - sq. in.

(10) v = velocity of fluid in the duct - ft./sec.

(11) v_o = velocity of fluid in entrance and exit pipes - ft./sec.

The loss in a pump where the cross-section changes from circular to rectangular and back to circular along with the reduc t ion and expansion of area, combined with the presence of the fringing magnetic field, would be greater than that occurring in a Venturi meter of nearly ideal shape. A value of 0.5 is suggested for K.

2) Calculation of Total Pressure Rise Necessary.

The pressure drops calculated for the duct and diffuser sections, when combined and added to the net pressure rise desired between the inlet and outlet of the pump will give the total pressure rise that must be developed in the duct.

3) Calculation of the Magnetic Field.

The magnetic fields of importance to the pump characteristics are the field crossing the duct between electrodes, and the fringing fields extending into the diffuser sections. These may be obtained by established procedures of magnetic circuit calculation. This involves a determination of the magnetic permeance of the gap across the duct between magnet poles, of the fringing flux paths across the diffuser section, of the fringing flux paths from the sides of the magnet poles, and of any other leakage flux paths in the magnetic circuit. These are important if a permanent magnet is used for excitation, in order to calculate the total flux being supplied by the magnet. Permanent magnet calculation procedures are described by Parker and Studders[2], Chapter 4. Chapter 5 of the same book describes procedures for calculating magnetic permeance of fringing and leakage flux paths. Roters[3], in his Chapter 5, also describes procedures for calculating magnetic permeance of fringing and leakage flux paths. Permanent magnet excitation is generally used only in small pumps. The fringing and leakage permeances are used in calculation of an electromagnet to obtain the total flux and the amount of magnetomotive force absorbed in the magnetic circuit.

The current between electrodes in the fluid and in the duct wall has a distorting effect on the magnetic field, increasing the field strength at the entrance to the duct and decreasing it at the exit end. This in turn affects the current distribution along the duct, producing maximum current density in the region of lower field strength and reducing the total pressure developed. Large pumps in which this effect is significant may be equipped with compensating conductors which return the current through the gap close beside its paths through the fluid and the duct wall, cancelling out most of the distortion. Equations are given by Blake[4] by which the effect on output pressure, output power, and electrical losses can be approximated for an uncompensated pump. These will be given in a following paragraph.

4) Calculation of Current, Voltage, Power and Efficiency

The equivalent circuit representing the d-c conduction pump, Figure II-102, is repeated below for easy reference, along with a tabulation of the nomenclature.

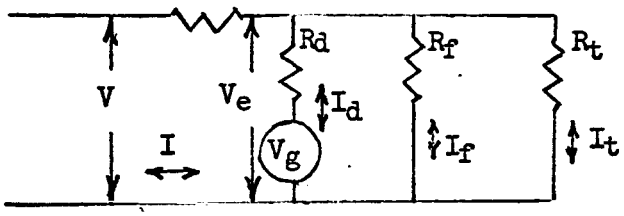

Figure II-102

D-C CONDUCTION PUMP EQUIVALENT CIRCUIT

R_e - Resistance of electrodes, electrode-to-duct-wall junction, duct wall thickness at the electrodes, the series magnet coil, and interconnecting bus.

R_d - Resistance of fluid directly between the electrodes.

R_f - Resistance of fringing current paths through the fluid.

R_t - Resistance of duct walls between electrodes.

I_d, I_f, I_t - Current in the respective branches R_d, R_f, and R_t

I - Total Current

V_g - Back emf generated by motion of the fluid

V_e - Voltage between duct wall inner surfaces at the electrodes

V - Voltage applied to the pump terminals.

Assume first that the pump is either of the permanent magnet type or is separately excited, so that the gap flux density is fixed and has been calculated as outlined in preceding paragraphs. Let P = pressure in psi developed in the pump, equal to the prescribed terminal pressure plus the hydraulic pressure loss which has been determined as above outlined. Let v = the velocity of flow in ft./sec. in the duct, calculated from the prescribed flow to be delivered by the pump at the prescribed pressure.

$$P = \frac{BI_d}{a} \times 8.85 \times 10^{-8} \text{ psi} \qquad (12)$$

B - lines/sq. in.

a - inches. duct height

b - inches. duct width

v - ft./sec.

$$I_d = \frac{Pa}{B} \times 0.1132 \times 10^{8} \text{ amp.} \qquad (13)$$

$$V_g = B\ v\ b \times 12 \times 10^{-8} \text{ volts} \qquad (14)$$

R_f - ohms

R_g - ohms

$$V_e = I_d R_d + V_g \text{ volts} \qquad (15)$$

R_d - ohms

$$I_f = \frac{V_e}{R_f} \text{ amp.} \qquad (16)$$

$$I_t = \frac{V_e}{R_t} \text{ amp.} \qquad (17)$$

$$I = I_d + I_f + I_t \text{ amp.} \qquad (18)$$

$$V = V_e + IR_e \text{ volts at terminals} \qquad (19)$$

$$W_i = VI \text{ watts input} \qquad (20)$$

(This does not include power for a magnetizing coil)

$$P_o = P - P_h \text{ psi output} \qquad (21)$$

$$W_o = P_o Q \times 0.435 \text{ watts hydraulic output} \qquad (22)$$

$$\eta = \frac{W_o}{W_i} \qquad (23)$$

(This does not include magnetizing coil power)

P_h - pressure loss psi

p - developed pressure, psi

Q - gal/min. flow

η - efficiency.

Calculation of R_d, R_f, and R_t is discussed in a following paragraph.

Consider now a series excited pump in which the gap flux density is proportional to the pump current.

$$B = CI \qquad (24)$$

$$I_d = \frac{Pa}{CI} \times 0.1132 \times 10^8 \text{ amp.} \qquad (25)$$

$$V_g = CI \text{ v b} \times 12 \times 10^{-8} \text{ volts} \qquad (26)$$

B - lines/sq. in.

I - amperes

C - Permenance constant determined in calculation of the magnetic circuit

V - ft./sec.

b - inches

a - inches

$$V_e = CI \text{ v b} \times 12 \times 10^{-8} + \frac{PaR_d}{CI} \times 0.1132 \times 10^8 \text{ volts} \qquad (27)$$

$$I = I_d + I_f + I_t \text{ amp.} \qquad (28)\ R_d,\ R_f,\ R_t \text{ ohms}$$

$$I = \frac{Pa}{CI} \times 0.1132 \times 10^8 + \frac{CIvb}{R_f} \times 12 \times 10^{-8} + \frac{PaR_d}{CIR_f} \times 0.1132 \times 10^8$$

$$+ \frac{CIvb}{R_t} \times 12 \times 10^{-8} + \frac{PaR_d}{CIR_t} \times 0.1132 \times 10^8 \text{ amp.}$$

(29)

$$I^2\left(1 - Cvb\left(\frac{1}{R_f} + \frac{1}{R_t}\right) \times 12 \times 10^{-8}\right) = \frac{PaR_d}{C}\left(\frac{1}{R_d} + \frac{1}{R_f} + \frac{1}{R_t}\right) \times 0.1132 \times 10^8$$

(30)

$$I = \sqrt{\frac{PaR_d\left(\frac{1}{R_d} + \frac{1}{R_f} + \frac{1}{R_t}\right) \times 0.1132 \times 10^8}{C\left(1 - Cvb\left(\frac{1}{R_f} + \frac{1}{Rt}\right) \times 12 \times 10^{-8}\right)}} \quad \text{amperes} \qquad (31)$$

Using above equations (25), (26), (27), (16) and (17), calculate I_d, V_g, V_e, I_f, I_t

$$V = V_e + IR_e \text{ terminal volts} \qquad (32)$$

$$W_i = VI \text{ watts input} \qquad (33)$$

$$P_o = P - P_h \text{ psi output} \qquad (34)$$

$$W_o = P_o Q \times 0.435 \text{ watts output} \qquad (35)$$

$$n = \frac{W_o}{W_i} \qquad (36)$$

The calculation of the resistances R_d, R_f, and R_t, is discussed by Blake[4] and Watt[5], and curves given to aid in the calculations. These curves are shown in Section II-A. They involve the assumptions that the duct is of uniform cross-section, rectangular in shape, and that the resistance is not affected by the presence of the magnetic field. It is assumed in applying these curves that the magnet poles extend over the

same axial length of the duct as the electrodes. The value of R_d is affected by the magnetic field in an uncompensated pump where the current distribution is changed by the field. A correction for this effect is given in a following paragraph. The value of R_f is affected by the fringing magnetic field which affects the fringing current distribution. It is also affected by the changing cross-section of the diffuser sections in which the fringing current paths lie; so that the value of R_f obtained from the curves is approximate. No suitable method of correction for these effects is available. The value of R_t is not affected by the magnetic field and is affected only slightly by changes in cross-section of the diffuser sections. The value of R_e depends upon the arrangement of the electrodes, the connecting buses, and the magnetizing coil, and can be calculated by established procedures. The contact resistance between the electrode and the duct wall depends upon the construction but is usually negligible. The above calculations for R_d and R_f assume good wetting of the duct wall by the fluid, with negligible contact resistance between the fluid and the wall. The resistance of the duct wall to the flow of current through its thickness from the electrode to the fluid may be conservatively approximated by assuming that all the electrode current flows straight through from electrode to fluid.

If fringe-current baffles are used in the pump to reduce the fringe current, the effective value of R_f is greater than would be obtained from the curves of Section II-A. The baffles are insulating plates placed in the diffuser sections parallel to the fluid flow but perpendicular to the fringe current flow, dividing the diffuser sections into two or more parallel channels. They may extend from the ends of the duct to the outer ends of the diffuser sections, or further, to reduce current flow around the outer ends. The value of R_t is not appreciably affected by the presence of the

baffles. The values of R_d and R_f may be approximated by using a value of b equal to the width of each separate parallel channel, calculating from Figure II-103 values of R_d and R_f for each channel, and adding together the values thus found to get the net effective value. Interchange of current between the fluid and the tube walls near the baffles is neglected.

5) Correction for Armature Reaction Effects

The distortion of the magnetic field and current distribution by the current in the fluid is discussed by Blake,[4] Watt,[5] Woodrow,[6] and Barnes.[7] Approximate corrections for this effect taken from equations developed by Blake are given here. The total developed pressure may be expressed as follows:

$$P = \frac{B_m I_d}{a} \left(1 - \frac{B_i}{B_m} \frac{\beta \coth \beta - 1}{\beta}\right) \times 8.85 \times 10^{-8} \text{ psi} \qquad (37)$$

$$R'_d = R_d \beta \coth \beta \qquad (38)$$

R_d = value of R_d as found from curves of Figure II-103

$$\beta = 1.915\ vc/10^7 \rho \qquad (39)$$

v = fluid velocity in the duct, ft/sec

c = electrode length along the duct, inches

ρ = electrical resistivity of the fluid, ohm-inches

B_m = average flux density across the duct between electrodes, lines per sq. in.

$$B_i = 3.19\ I/2d, \text{ lines per sq. in.} \qquad (40)$$

d = gap between magnet poles, inches

I = total electrode current, amperes

B_i is the value of the flux density at the edges of the magnet poles, (at the entrance to and exit from the duct), which would be produced by the current through the magnet gap alone. Strictly speaking, the current

I should include only I_d and the portion of duct wall current between the poles. The overall accuracy of the correction, however, does not warrant the extra calculation to obtain these values.

B_m may be obtained by assuming that the distortion of current distribution does not affect the total flux and making the calculation as if the current distribution were not distorted. The total electrode current may be assumed to flow in a half turn adding to or subtracting from the external gap magnetomotive force, depending upon the geometry of the electrode connections. This is an approximation as the distortion of current distribution will affect the total flux.

Plots of $\beta \coth \beta$ and of $\frac{\beta \coth \beta - 1}{\beta}$ are given in Figure II-103 as functions of β to assist in determining the correction factors.

For series electromagnet pumps the ratio of B_i/B_m is nearly constant

$$\frac{B_i}{B_m} = \frac{3.19I/2d}{CI} = \frac{1.59}{Cd} \qquad (41)$$

$$\text{Let } X = \left(1 - \frac{B_i}{B_m} \frac{\beta \coth \beta - 1}{\beta}\right) = \left(1 - \frac{1.59}{Cd} \frac{\beta \coth \beta - 1}{\beta}\right) \qquad (42)$$

$$\text{Let } P' = P/X \qquad (43)$$

Then equations (24)-(36) may be used to include the effects of armature reaction by substituting P', (43), and R'_d, (38) for P and R_d.

For permanent magnet or separately excited pumps B_m is constant, but B_i varies with current. It is necessary to first calculate the currents as if there were no armature reaction, obtain an approximate value of Bi and of X, then repeat with P' and R'_d. It may be necessary to then revise the values of B_i, X, and P' and again repeat the calculation.

REFERENCES

1. Mechanical Engineers Handbook, 5th Ed., Lionel S. Marks, McGraw-Hill Book Co.

2. Permanent Magnets and Their Application, Parker and Studders, John Wiley and Sons, Inc.

3. Electro-Magnetic Devices, Roters, John Wiley and Sons, Inc.

4. Conduction and Induction Pumps for Liquid Metals, L.R. Blake, Proceedings IEE, Vol. 104, Part A, 1957.

5. The Design of Electromagnetic Pumps for Liquid Metals, D.A. Watt, Proceedings IEE, Vol. 106, Part A, 1959.

6. The D-C Electromagnetic Pump for Liquid Metals, J. Woodrow, A.E.R.E., E/R 452.

7. Direct Current Electromagnetic Pumps, A.H. Barnes, Nucleonics, January 1953.

APPENDIX II

DESIGN DATA BOOK ADDITION

SECTION III

MATERIALS AND PROCESSES

The heat transfer design approach for polyphase induction pumps as shown in Section VII calls for a gas filled stator cavity. Choice of gases for this application requires attention to thermal conductivity, dielectric strength and chemical stability in the expected environment. Helium being the obvious choice from the view of thermal conductivity and stability its dielectric strength was investigated first and some comparisons to other gases made as presented below.

The investigation was based on the following design conditions:

(a) Enclosure is to be filled to one atmosphere of pressure at room temperature.

(b) Maximum temperature of stack, conductor and gas is expected to be 800°F.

(c) Minimum separation of conductors is .010 inch, conductor coated with glass roving, ceramic particles, ceramic "film" or other insulating material.

(d) Radiation: 10^7 Rads; 10^{12} to 10^{14} NVT.

The locations of particular concern are the slots where turn, phase, and coil to ground voltages may exist, and at end loops close to each other. From a thermal conductivity standpoint, helium is good; but of the commonly available gases on which dielectric information is readily available, it is the poorest electrically. At the pressure and gaps indicated, the DC sparkover voltages are as shown in G. A. Farrall's survey of Paschen curve information, Research Lab. Memo-Report P215, dated December, 1959:

Gas @ 760 Torr @ R.T.	Volts .010" Gap	.002" Gap	.001" Gap
Helium	350	210	280
Neon	360	250	260
Argon	590	290	270
Hydrogen	950	400	310
Air	1700	620	450

Also, see attached curve from R.L. Memo Report P-215.

It must be emphasized that these values are for: (1) uniform electrical field, (2) the gas only, and (3) DC voltages.

For small gaps only small errors are incurred by considering the DC value as peak AC value. Somewhat larger variations may occur with different electrode materials, at this and smaller pressure and gap distance products. Oxode and other coatings on electrodes usually reduce the sparkover values. However, very significant reductions may result from the following:

(a) Non-uniformity of field: In most electrical equipment a non-uniform field is usual. The EM pump is likely to be no different. A reduction of 30% in the above values is not unusual.

(b) Interposed material in the gap: No serviceable high temperature conductor insulation of a truly film nature, similar to Formex for low temperature, is known. Even chemically formed oxide films do not ensure a completely unbroken film. Whether the conductors are spaced by oxide film, by attached ceramic granules, or by inorganic fibers, such matter represents an interposed material of higher dielectric constant between the electrodes. It is uncertain at the moment if these should be calculated as equivalent to an interposed film plus gas gap in series or as equivalent to a shunting

surface between electrodes. In either case there is some probability of overstressing the gas to cause corona or breakdown. Estimated reduction of flashover voltage for this cause is a minimum of 30%.

(c) Radiation: Although helium (and nitrogen) per se are not subject to damage at the radiation fluxes involved, the gap flashover voltage will likely be somewhat lower because of the high irradiation of the gap and electrode materials.

(d) Impurities in the gas: The nature of the impurity(ies) governs whether the breakdown voltage is increased or decreased. Most impurities degrade the dielectric properties.

The conclusion is that in helium, turn to turn breakdown, etc. is likely not to exceed 50 V RMS 60 cy. This appears to be very marginal. In the case of solid material slot liners the division of voltage between solid and possible gas gaps appears to be less disadvantageous, but still may be considered marginal. Even if non-porous separators between phase or other conductors in the same slot or external to slots are capable of withstanding corona attack, corona effects on the inevitable impurities in the enclosed atmosphere may have deleterious effects; and, certainly corona or sparking is undesirable from a communications standpoint.

Possible Solutions:

Several solutions immediately suggest themselves.

(a) Increase the gap.

(b) Increase the filling pressure.

(c) Add other gases to improve the dielectric properties with minimum interference with heat transfer.

(d) Combinations of above.

The first two, within reasonable limits, will increase the breakdown strength but not in direct ratio; see curves, Figure 10. The third possible solution requires examination. The approximate improvement possible with the addition of nitrogen or octofluoropropane (C_3F_8) to helium is indicated in the attached graph. The crux of the situation is the possibility of radiation damage to the gas and consequent deterioration of properties or attack on other materials. Sulfur hexafluoride (SF_6) addition would appear to be suitable from dielectric and thermal conductivity standpoints, but SF_6 is believed to be sufficiently radiation sensitive to be unsuitable. In addition, the expected 800°F is uncomfortably close to the start of dissociation (450°C). Heavier gases which might be more desirable from the standpoint of dielectric and thermal conductivity properties are also more complex and usually more subject to radiation damage. C_3F_8 has been suggested by Sharbaugh at Research Lab as possibly radiation suitable. CF_4 (Freon 14) has been suggested by Dutton of Medium Transformet Dept. as another possibility on the basis that it is a saturated compound. Insufficient evidence is at hand at the moment to draw sound conclusions about any of the additions other than nitrogen.

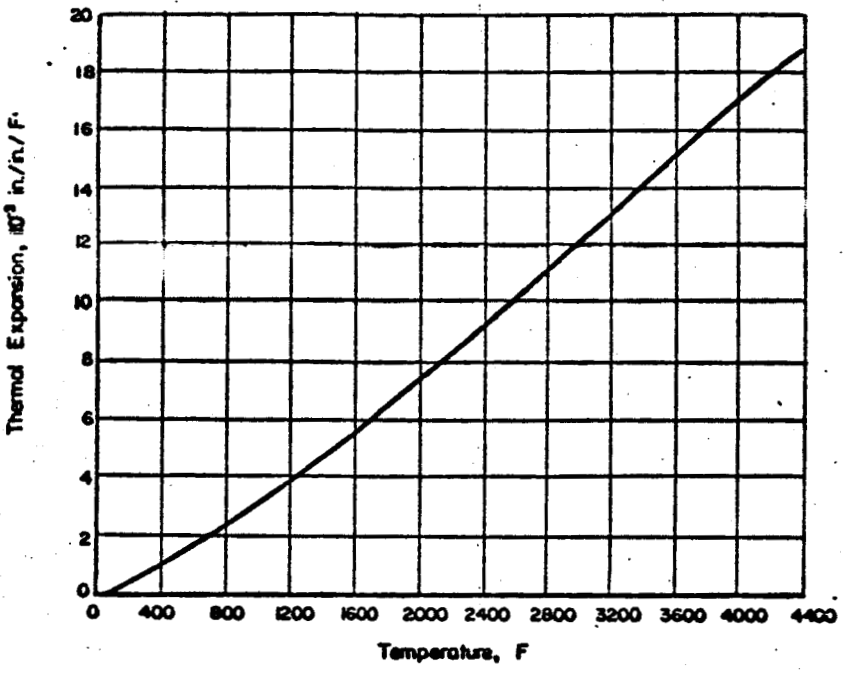

FIGURE A-50. THERMAL EXPANSION OF T-111[2]

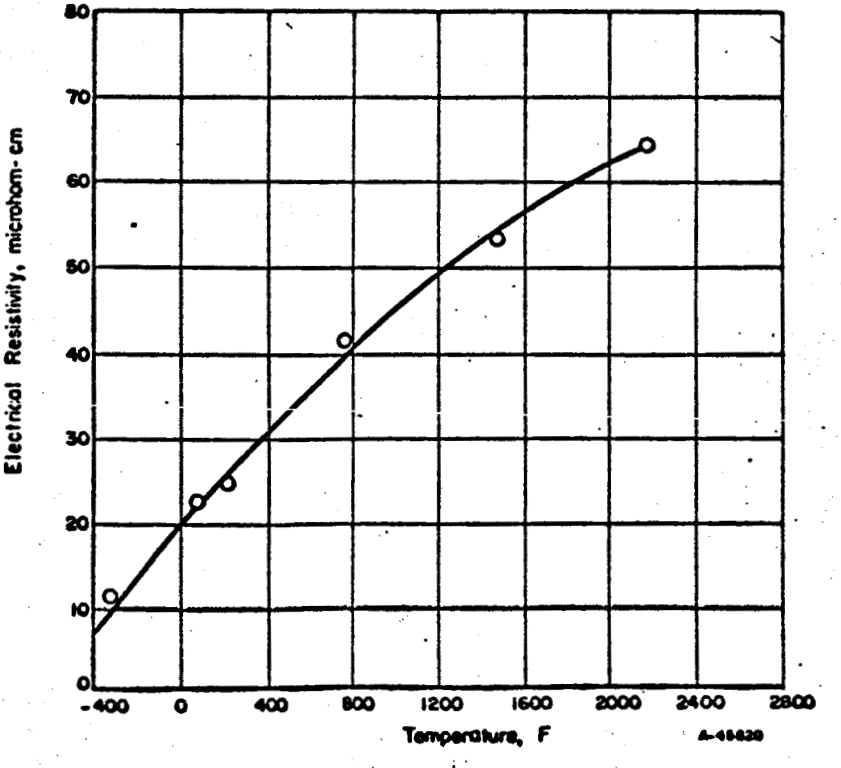

FIGURE A-51. ELECTRICAL RESISTIVITY OF RECRYSTALLIZED T-111[2]

TABLE A-43. STRESS-RUPTURE PROPERTIES OF ARC-CAST T-111 SHEET AT 2400 F

Condition	Stress, 1000 psi	Time to Rupture, hours	Elongation, per cent	Reference
Stress-relieved sheet (3 hr 2250 F, 0.040 inch)[a]	35.0	0.5	--	(3)
	33.0	0.8	--	
	30.0	7.3	--	
	25.7	5.0	--	
	23.0	5.0	--	
	20.0	19.8	--	
Stress-relieved sheet (reduced 65 per cent, 1 hr 2000 F)[b]	30.0	2.3	56	(1)
	25.0	4.3	58	
	20.0	25.7	94	
Recrystalled sheet (reduced 80 per cent, 1 hr 3000 F)[b]	30.0	3.0	30	(1)
	25.0	7.3	40	

(a) Analyses 7.8% W, 1.95% Hf, 0.0027% C, 0.0023% O, 0.0026% N, 0.0035% Fe, 0.0008% Cr, 0.0005% Ni, and 0.0100% Mo.

(b) Low interstitial grade.

SECT. IIIB, MATERIALS
DUCT MATERIALS
TANTALUM ALLOYS
COMPARE 133

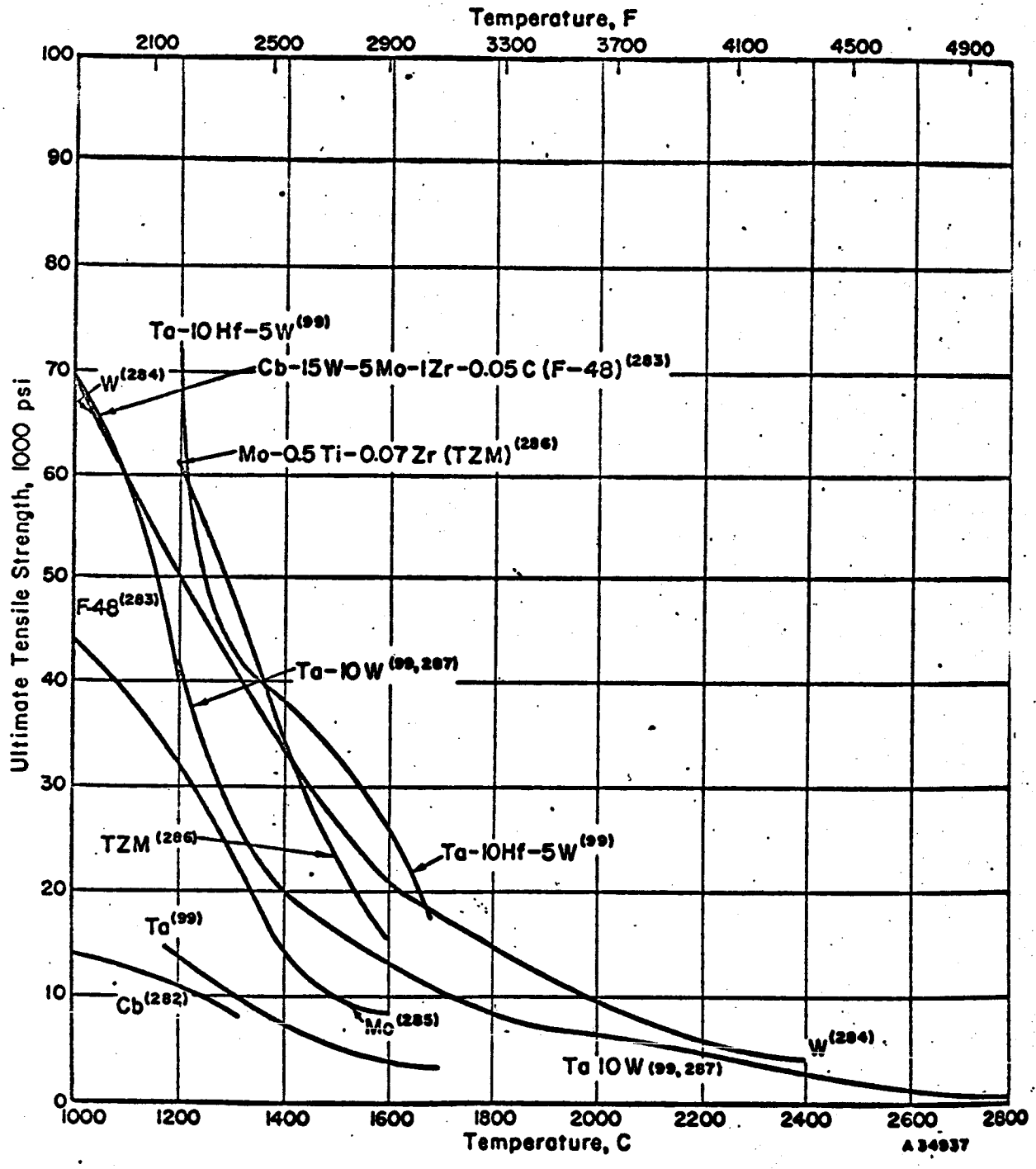

Ultimate Tensile Strength, 1000 psi / Density, lbs/in.³

FIGURE 163. EFFECT OF TEMPERATURE ON THE ULTIMATE TENSILE STRENGTH OF SELECTED REFRACTORY METALS AND ALLOYS

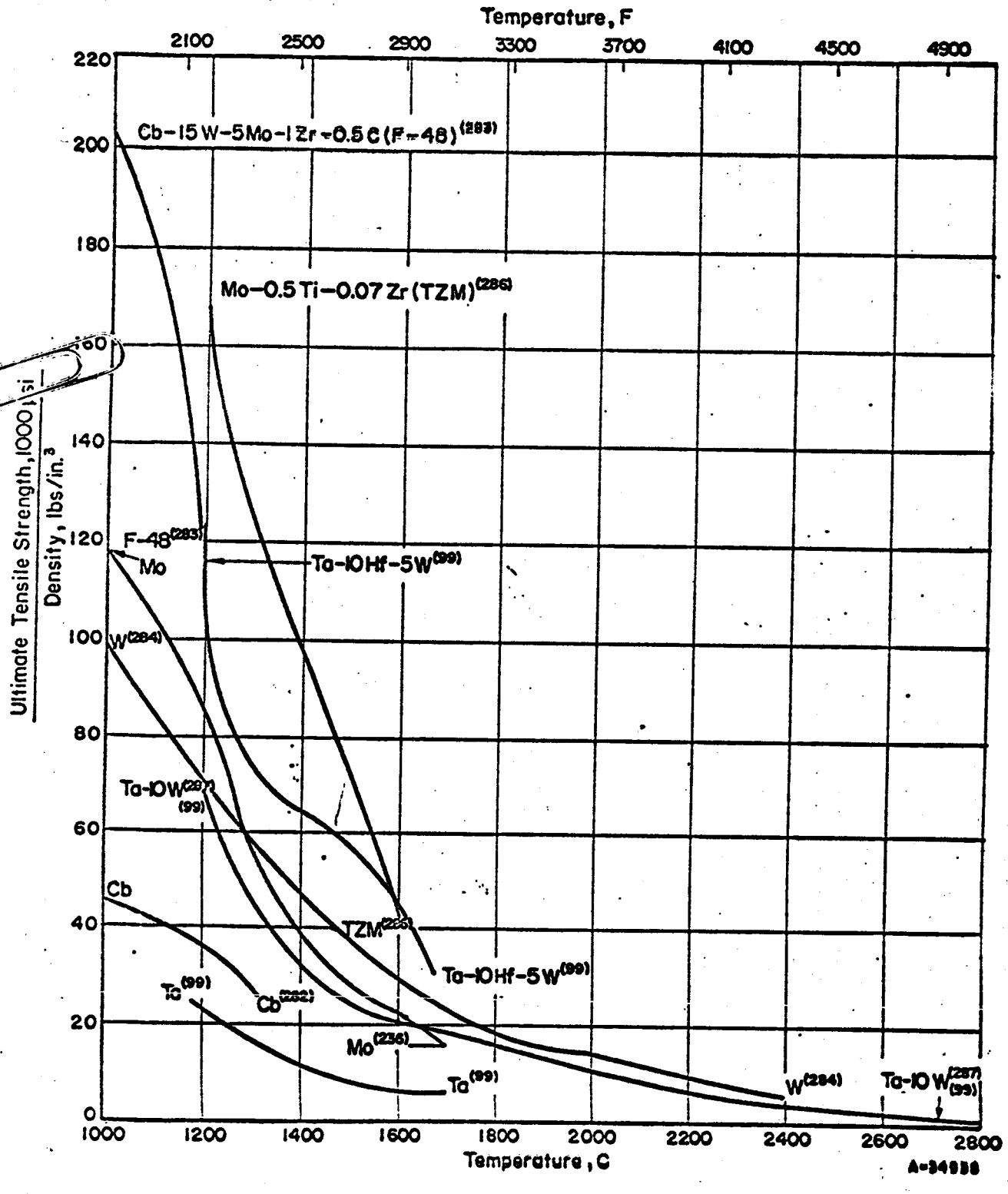

FIGURE 164. EFFECT OF TEMPERATURE ON THE ULTIMATE TENSILE STRENGTH/DENSITY OF SELECTED REFRACTORY METALS AND ALLOYS

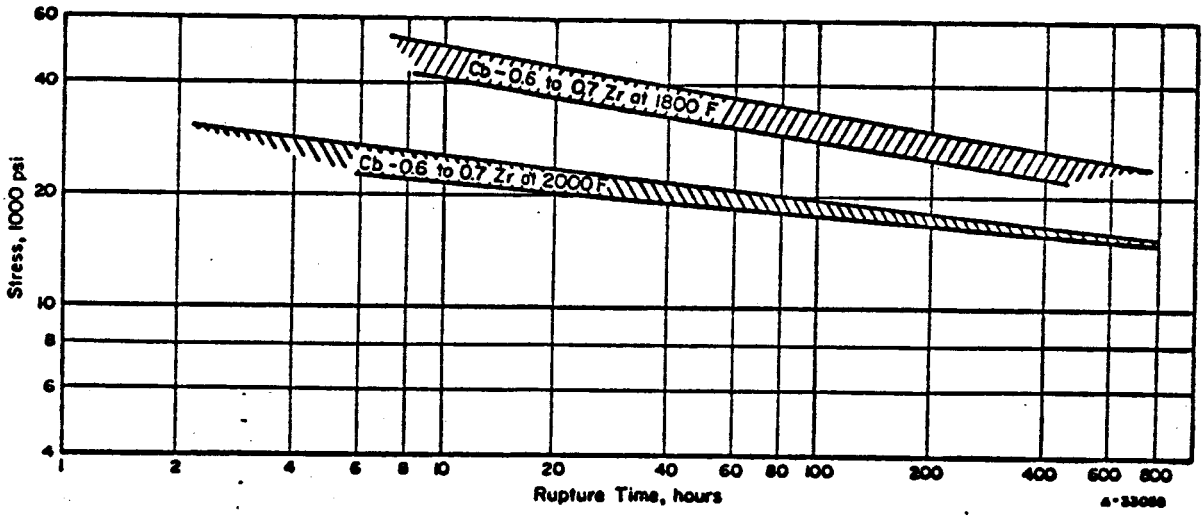

FIGURE A-35. STRESS-RUPTURE PROPERTIES OF Cb-1Zr AT 1800 AND 2000 F(9)

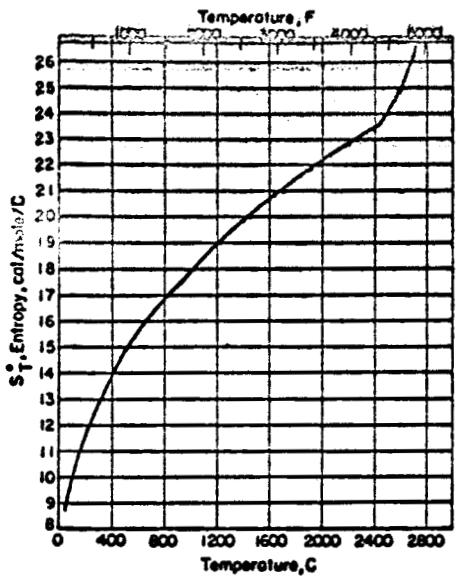

FIGURE 5. ENTROPIES OF COLUMBIUM FROM 25 TO 2727 C[14]

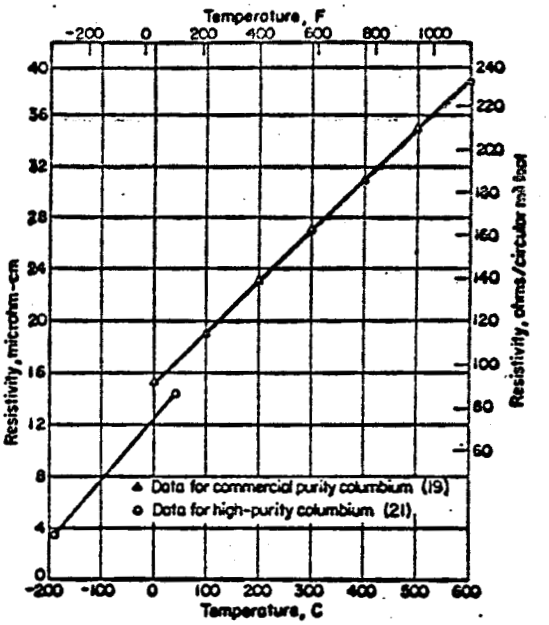

FIGURE 6. ELECTRICAL RESISTIVITY OF UNALLOYED COLUMBIUM

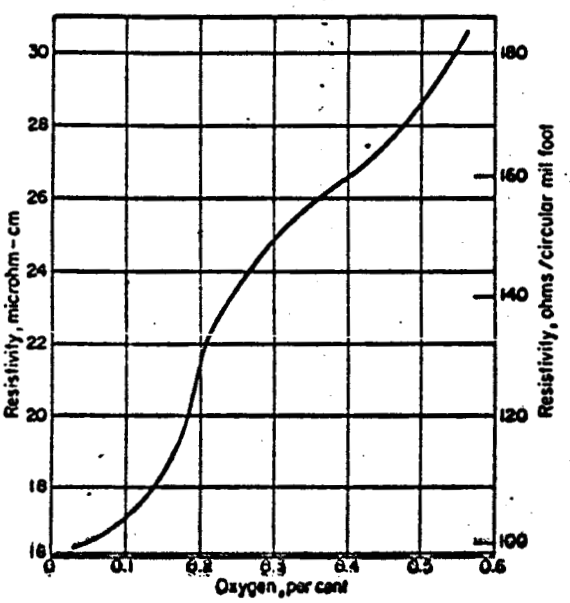

FIGURE 7. EFFECT OF OXYGEN ON THE ELECTRICAL RESISTIVITY OF COLUMBIUM AT ROOM TEMPERATURE[19]

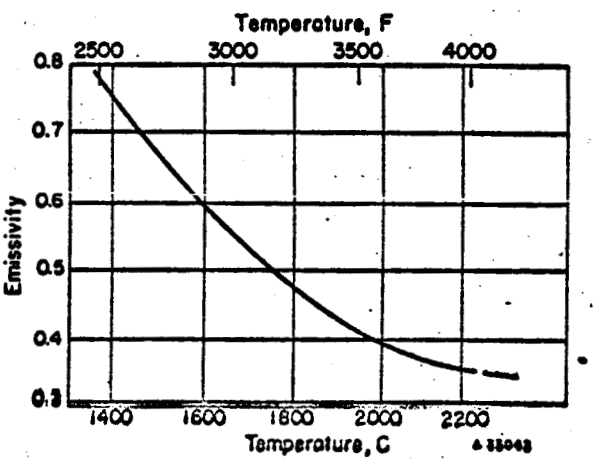

FIGURE 8. EFFECT OF TEMPERATURE ON THE EMISSIVITY OF COLUMBIUM[26]

λ = 6500 A

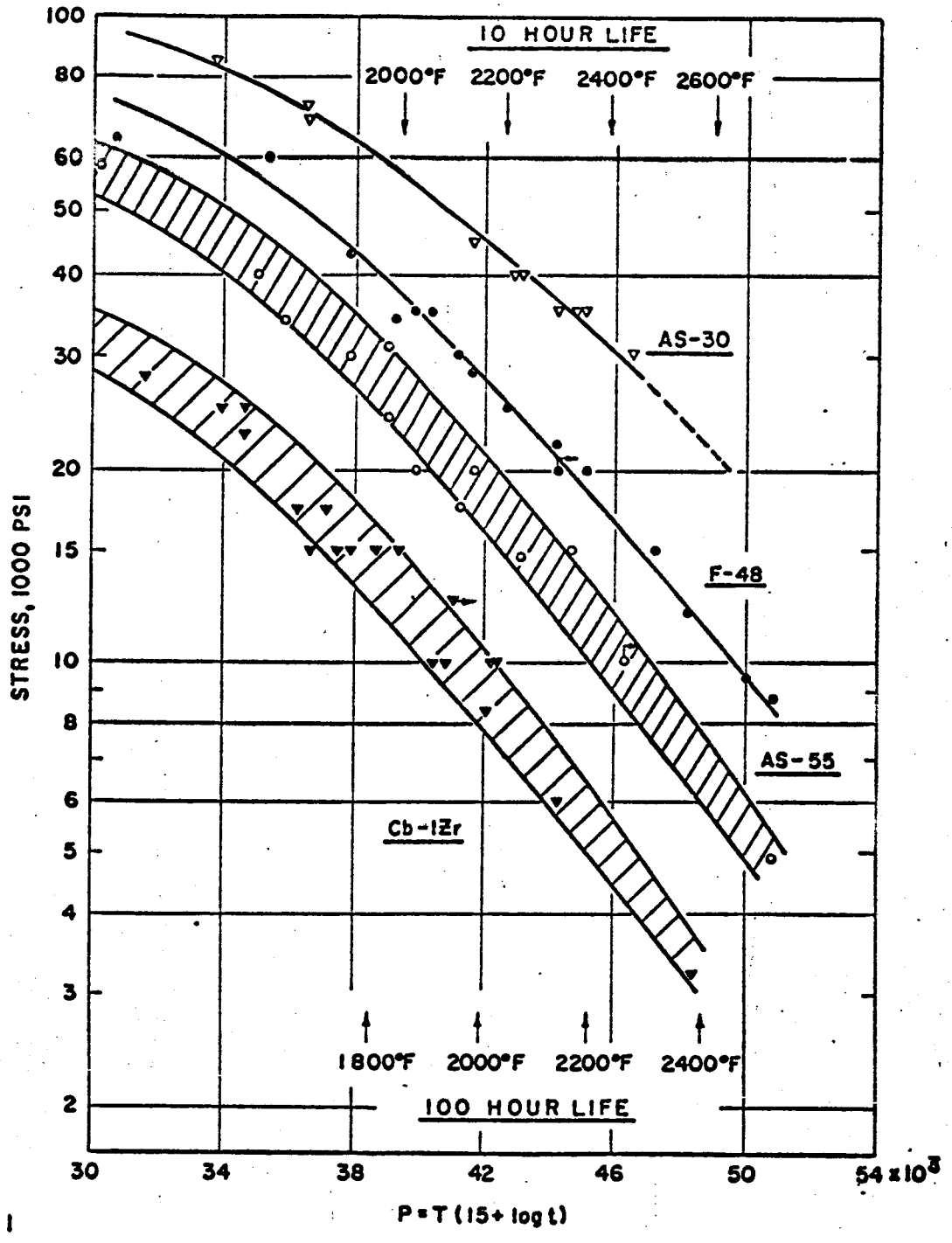

Figure 7. Stress-Rupture Properties of Wrought and Stress-Relieved Cb-Base Alloys.

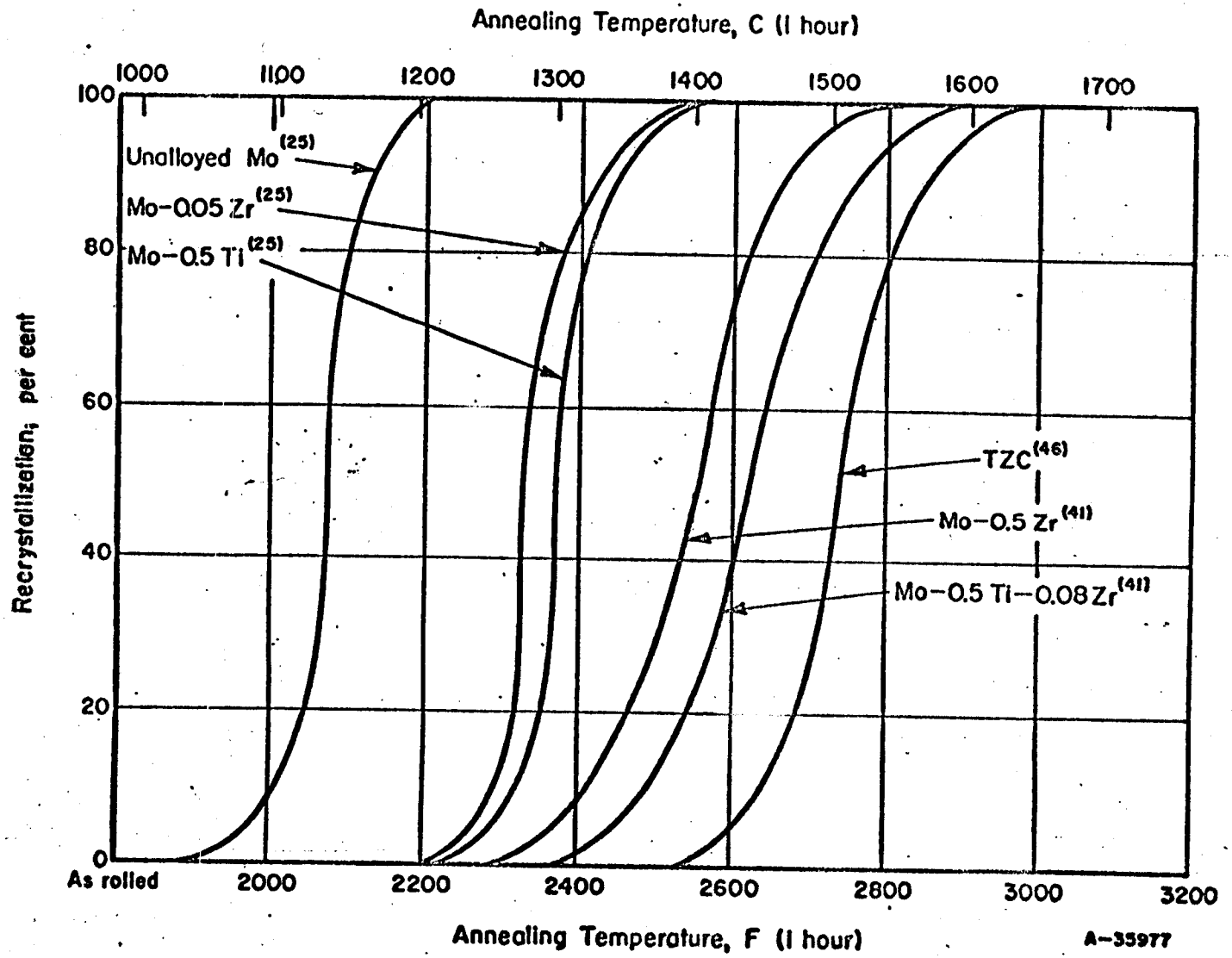

URE 72. EFFECT OF ANNEALING TEMPERATURE ON THE RECRYSTALLIZATION OF MOLYBDENUM-BASE ALLOYS

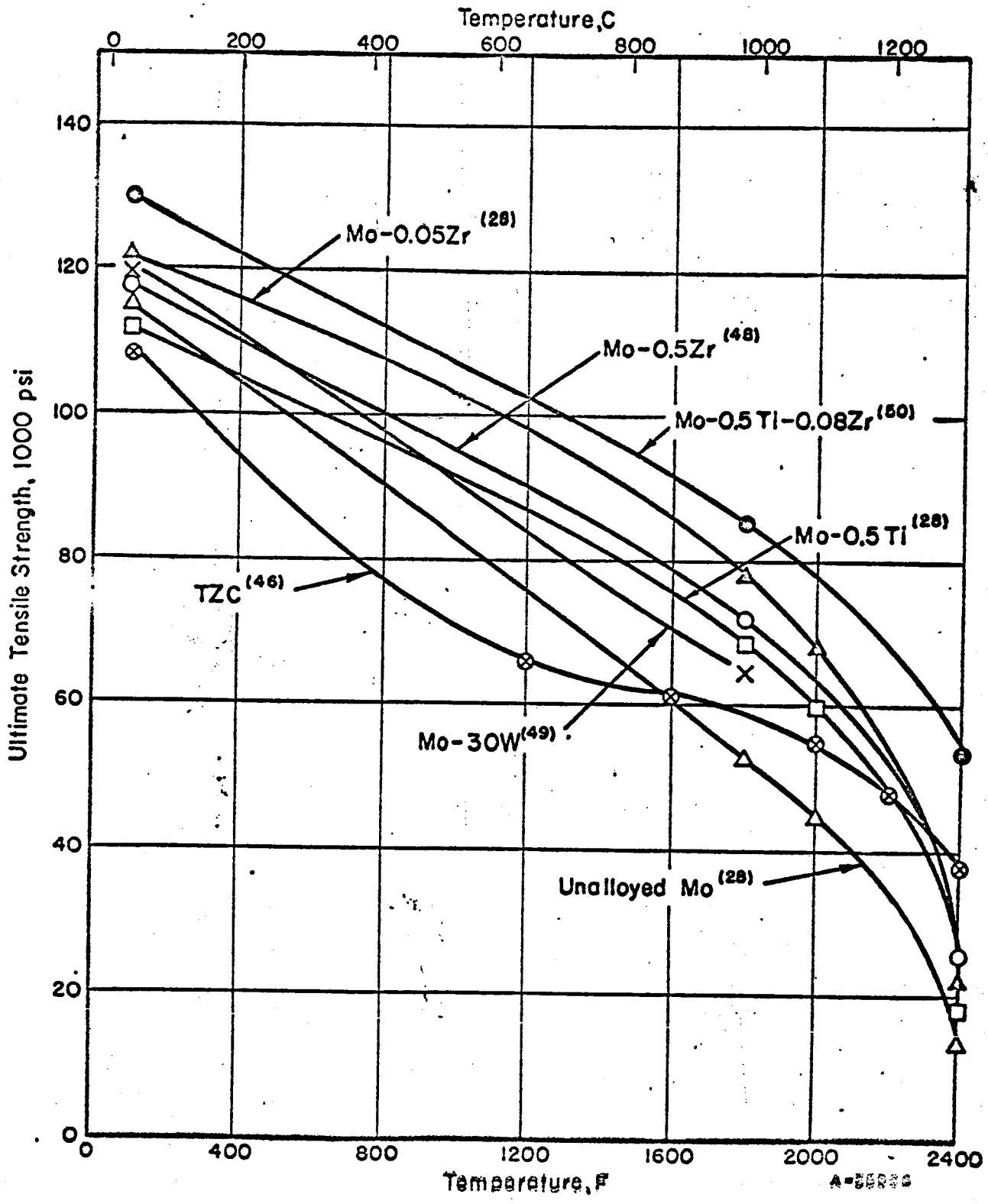

FIGURE 81. TENSILE STRENGTH-TEMPERATURE RELATIONSHIP FOR SELECTED MOLYBDENUM-BASE ALLOY BAR STOCK IN THE STRESS-RELIEVED CONDITION

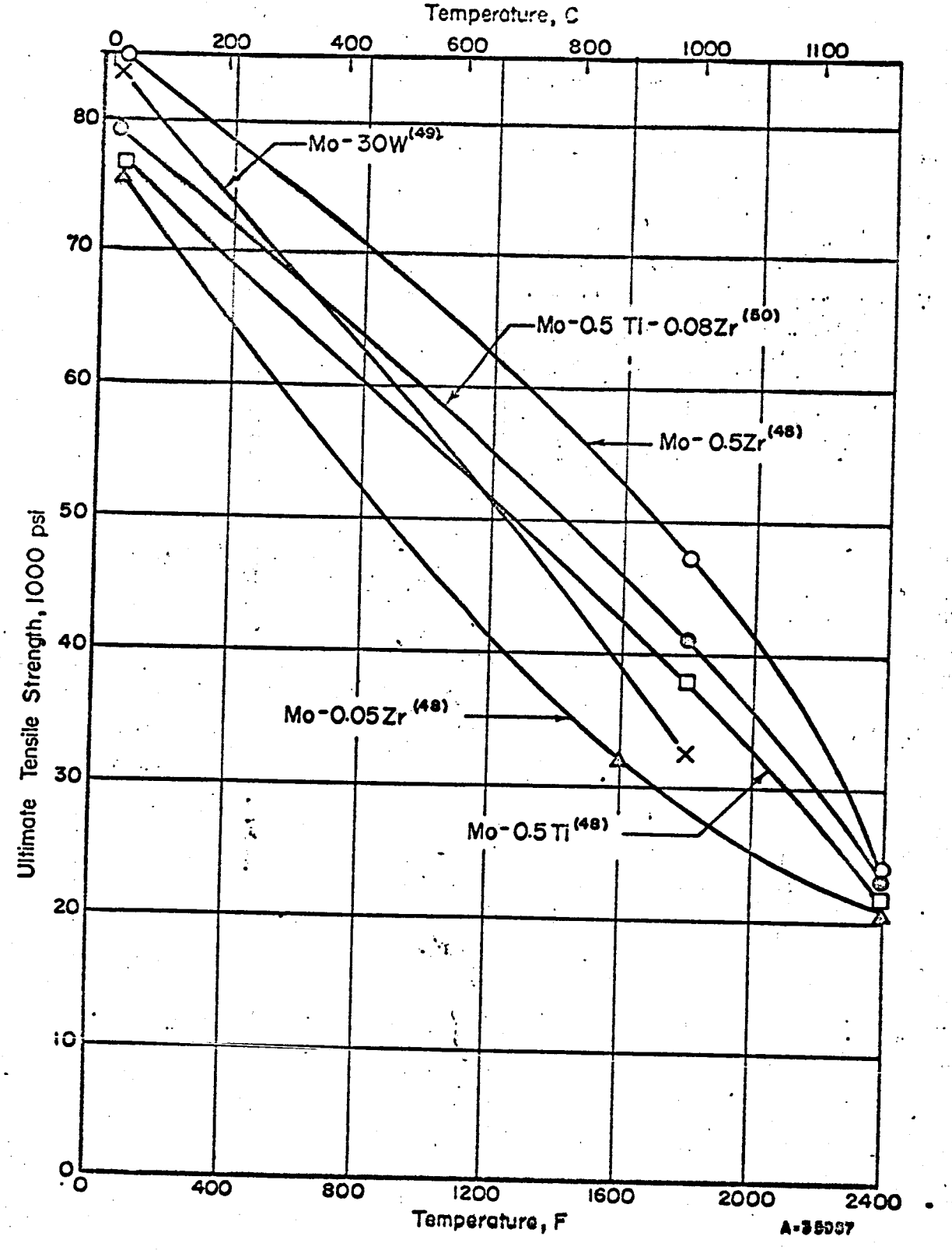

FIGURE 82. TENSILE STRENGTH-TEMPERATURE RELATIONSHIP FOR SELECTED MOLYBDENUM-BASE ALLOY BAR STOCK IN THE RECRYSTALLIZED CONDITION

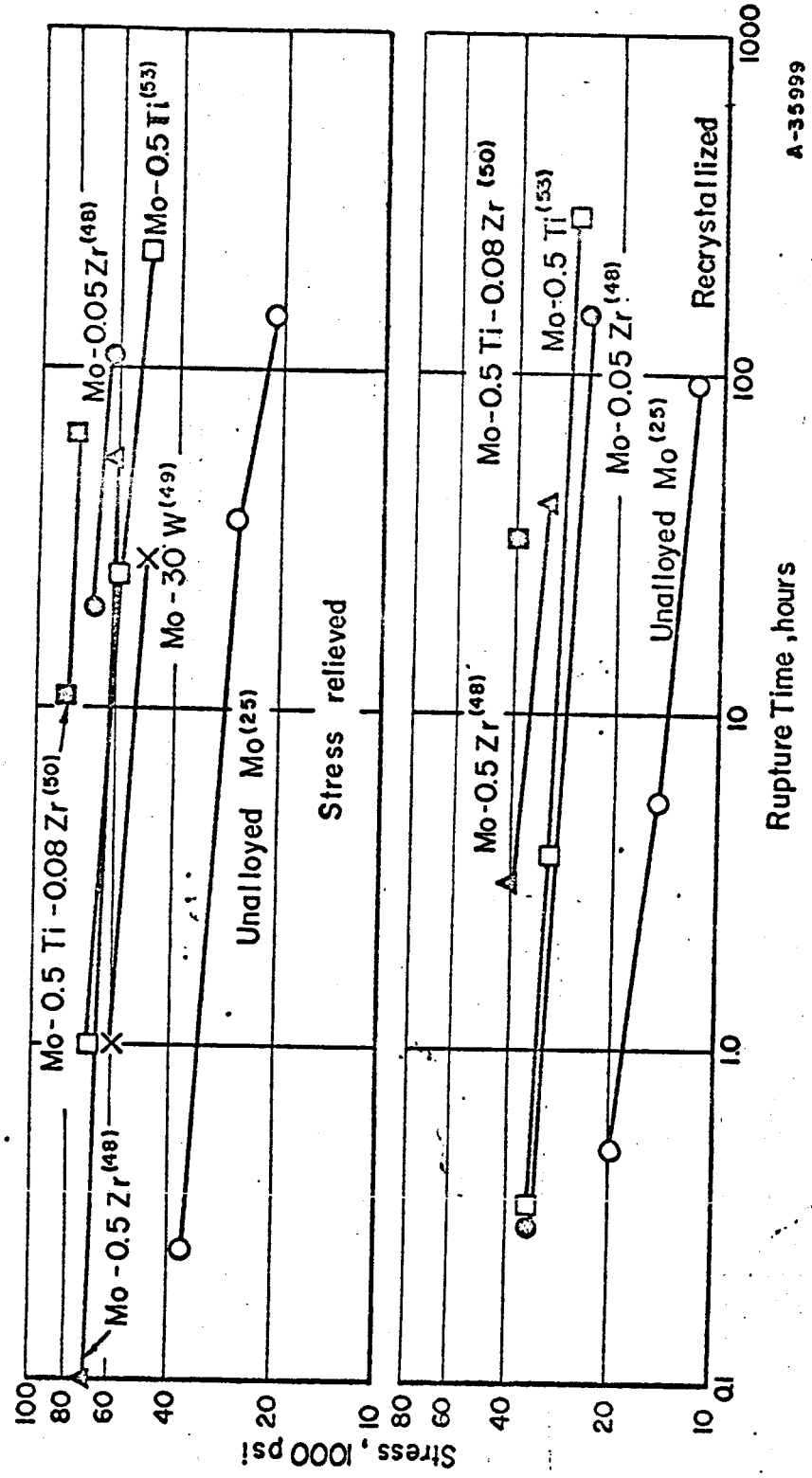

FIGURE 94. STRESS-RUPTURE CURVES FOR SELECTED MOLYBDENUM-BASE ALLOYS TESTED IN THE RECRYSTALLIZED AND STRESS RELIEVED CONDITIONS 1800 F

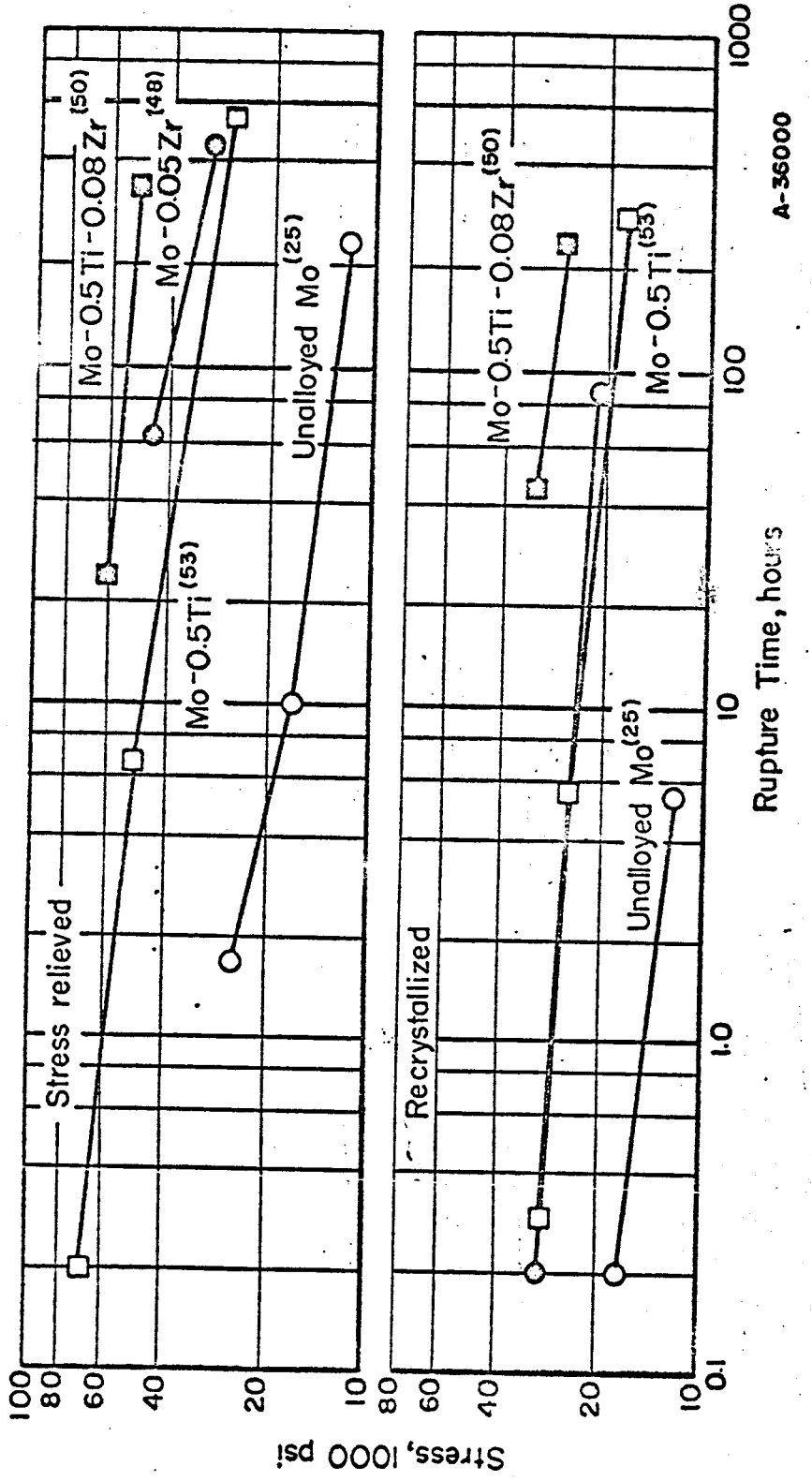

FIGURE 95. STRESS-RUPTURE CURVES FOR SELECTED MOLYBDENUM-BASE ALLOYS TESTED IN THE RECRYSTALLIZED AND STRESS-RELIEVED CONDITIONS AT 2000 F

APPENDIX III

DESIGN DATA BOOK ADDITION

SECTION VII

EM PUMP SELECTION AND DESIGN

A. TURBOELECTRIC POWER PLANT APPLICATIONS

1. General

As a trial of EM pump application in the turboelectric plant several preliminary polyphase induction designs were made. The polyphase pump was selected since the frequency changer is inherently more reliable and lower in weight than rectification equipment. This may be seen by comparing the weights presented for the power conditioning systems in Section V "Power Supply". As described below a helical induction pump was chosen for the potassium condensate boost application whereas an annular linear type was selected for the lithium radiator coolant pump.

2. Condensate Boost Pump

The design point rating for the condensate boost pump in the turboelectric power plant is 1.5 lb/sec. 1200°F potassium at 100 ft. head with a 10 ft. NPSH.

At the design point rating the helical induction pump is best suited to the application, since the flow is low and the pressure rise is relatively high. Several preliminary designs were laid out for frequencies of 50 and 100 cps and performance was calculated. The curves of Section II were applied in selecting the best pump configuration for analysis. The curves indicate that in the 50-100 cps frequency range the best efficiency will be attained at 50-60% slip.

One of the best designs considered is illustrated in Figure VII-3. Calculated performance of this design is listed below:

Pump	
Power Input	1.6 KW
Power Factor	0.5
Efficiency	0.127
Power Frequency	100 cps
Weight	35 lbs.

Pumping System Weight	
4 pumps	140
Power Penalty @ 10 lb/KW	64
Frequency Converter @ 2 lb/KW	12.8
TOTAL	217 lb.

Note: Weight penalties for cooling and for low power factor not included.

Performance was calculated by the General Electric Company proprietary program for helical EM pump design, which is based on the fundamental relationships to be given in Section II. The approach to heat transfer given in Section II was used in that the pump windings are assumed to be contained within an hermetically sealed envelope enclosing helium at 1 atmosphere. Although no specific winding temperature calculations have been made, the calculated winding current density is 4926 amp/in^2, a value which appears reasonable, on the basis of experience with machines of this general size.

Duct design is such that pump entry and exit are at the same end of the pump, and there is no mechanical connection between the duct and the stator structure. Thermal insulation between pump duct and stator structure is exposed to the vacuum of space and may be any of a variety of materials as, for examples, dimpled stainless steel strip or alternate layers of stainless steel strip and stainless steel wire cloth. A radial space of 0.040" has been allowed for thermal insulation. Pump flow is by way of two parallel passages, each of square cross-section with 0.315" length of side. Flow velocity is about 25 ft/sec., giving a velocity head of 9.8 ft.

The pump operates on 60 cycle 3 phase power. In all analyses, the calculated optimum frequency assumed a value between 50 and 100 cps. For obvious convenience in testing, 60 cps is stipulated here. The pump, a two pole machine operating at approximately 50% slip at design point, uses 1.6 kw power input at 0.5 power factor. The over-all efficiency is approximately 13%.

The illustration of Figure VII-3 depicts the entry flow direction into the inlet pipe, which is connected to the plenum chamber of the pump duct. The flow path is then through the helical passages, where the pumping force is applied. The flow exits through the center pipe at a 180° angle to the inlet flow.

The magnetic core is laminated sheet. The material selected, usually adequate for applications to 1700°F, is a cobalt iron to permit heat rejection to the 1200°F fluid passing through the exit pipe. These temperatures are marginal for the conventional electrical steels.

The system requirements will prescribe the duct material. Based on the flight design, a columbium alloy with 30 to 40 mil thickness is currently being deliberated for the containment walls. In testing, to avoid the problems of refractory metal alloys, an alternate material should be considered. If stainless steel is chosen, some improvement in performance can be anticipated because of its higher resistivity. To reduce the heat flow to the stator, thermal insulation is applied to the exterior of the duct. The insulation comprises multiple layers of metal foil, preferably stainless steel.

The stator will be cooled by the 600°F liquid metal flowing through coolant tubing which is brazed to the stator casing. This would be part of the same coolant system provided for bearings, seals and generator cooling in the turboelectric

power plant. The resultant hot spot temperature is estimated at 800°F. Consequently, stator materials have been selected to accommodate these requisities. The laminations are low silicon iron. Copper conductors will be insulated with served glass and impregnated with aluminum phosphate. To ensure that heat generated in the windings is conducted uniformly to the stator and finally to the coolant, the frame is designed to form a gas tight envelope around the stator. The cavity is filled with nitrogen as a heat transfer agent. From the thermal conductivity view, helium would be desirable but its dielectric strength may be too low.

The stator frame is a stressed skin design fabricated from stainless steel, contains the nitrogen, and provides a support structure for the pump.

The entire pump might be enclosed in a secondary shell which would provide additional protection and a guard against loss of nitrogen.

3. Lithium Radiator Coolant Pump

The design point specified for the radiator coolant system using lithium at 1200°F is 2 lb/sec at 20 psi pressure rise. A total of 16 such pumps would be used for a 16 circuit radiator. This flow-head combination does not present a clear choice of pump type. A helical design is presented below under 4. Other types including a single phase design will be investigated. However, the alternate arrangement using 4 pumps of 8 lb/sec flow rate and 20 psi head permits effective employment of the annular linear induction pump. The resultant pumping system has more attractive weight and efficiency characteristics.

A set of calculations was run and a pump design worked out. The design is depicted in Figure VII-4. Materials choices and the general design

approach is the same as for the condensate boost pump. The calculated performance is:

Pump	
Power Input	6 KW
Power Factor	0.53
Efficiency	0.15
Frequency	50 cps
Weight	85 lbs.

Pumping System Weight	
4 Pumps	340 lb.
Power Penalty @ 10 lb/KW	240
Frequency Converter @ 2 lb/KW	48
TOTAL	628

Note: Weight penalties for low power factor and cooling not included.

Performance was calculated using a computor program for linear induction pump design, which is based on the fundamental relationships now under development as reported in Section II-A. The winding cavity was assumed to be sealed and to contain helium at about 1 atmosphere. Current density in the winding is about 5120 amp/in.^{2}, which is reasonable. Detailed heat transfer and temperature distribution calculations have been made.

The duct is mechanically simple and free of stress problems. A straight through arrangement is illustrated, flow enters one end of the pump and out the other. It may be possible to develope a reverse flow arrangement in which pump entry and exit are at the same end of the pump. The duct itself is annular, with axial flow at a velocity of 20 ft/sec. As in the case of the condensate boost pump described in another section of this report, the thermal insulation in the space between the pump duct and the pump stator is exposed to the vacuum of space. Here again a metallic insulation system appears feasible. Other materials choices and design details are also similar to the boost pump.

4. Alternate Designs

For purposes of comparison several alternate pumps were considered for the radiator coolant applications. Rough estimates of the characteristics for these pumps were made and are shown below.

a) NaK Radiator - 16 Annular Induction Pumps

Pump		Pumping System Weight	
Weight	85 lbs.	16 Pumps	1360 lb.
Power Input	6 KW	Power Penalty	960
Efficiency	11 %	Power Conditioning	192
Power Factor	.51	TOTAL	2512

b) Li Radiator - 16 Annular Induction Pumps

Pump		Pumping System Weight	
Weight	40 lbs.	16 Pumps	640 lb.
Power Input	2.2 KW	Power Penalty	350
Efficiency	12 %	Power Conditioning	71
Power Factor	.51	TOTAL	1061

c) Li Radiator - 16 Helical Induction Pumps

Pump		Pumping System Weight	
Weight	48 lbs.	16 Pumps	768 lb.
Power Input	2.2 KW	Power Penalty	350
Efficiency	12 %	Power Conditioning	71
Power Factor	.70	TOTAL	1189

Obviously from the optimum pumping system viewpoint, lithium is clearly the preferred radiator coolant. However, it is important to note the weight advantage indicated in using a smaller number of large pumps. In a manner similar to most electrical machinery both specific weight and efficiency improve with size. Also the interplay between efficiency, weight

and power factor can be seen in comparing the condensate boost pump with the helical induction pump for lithium radiator application.

5. Boiler Feed Pump

Although not specifically named in the work statement a boiler feed pump application looks very promising for the Rankine cycle turboelectic system. This installation would be the prime-mover for the condensate to the boiler and would replace the earlier concept of a canned rotor pump and EM pump booster combination.

In analyzing the boost pump described above it became evident a helical induction EM pump could readily perform the complete task of feeding condensate to the boiler. A supplementary boost pump would be precluded and the highly reliable induction EM pump would be applied to the entire pumping job.

The pump requirements were derived from the flow specified for the boost application plus the boiler pressure demands of a typical turbogenerator power plant. Consequently, the design point selected was 15.5 gpm at 100 psi developed head. The resultant design is illustrated in Figure VII-5. The diameter is 6.5 inches; the length, 21 inches; the total weight, 105 pounds. Again, 3 phase 60 cycle power is employed. The pump, a two pole machine, uses 5 kw of power at 50% power factor with a 50% slip. Over-all efficiency is approximately 12%.

Those materials selected for the two preceding designs are used here. Generally, the arrangement and configuration approximate those of the boost pump. The inlet nozzle design, however, has been improved hydraulically.

The flow exit from the helical section is cleaner, the end turns have been shortened, and concurrently, the stator cavity has been reduced. To provide a secondary barrier against leakage, the thermal insulation is completely canned.

CONDENSATE BOOST PUMP TURBOELECTRIC SYSTEM

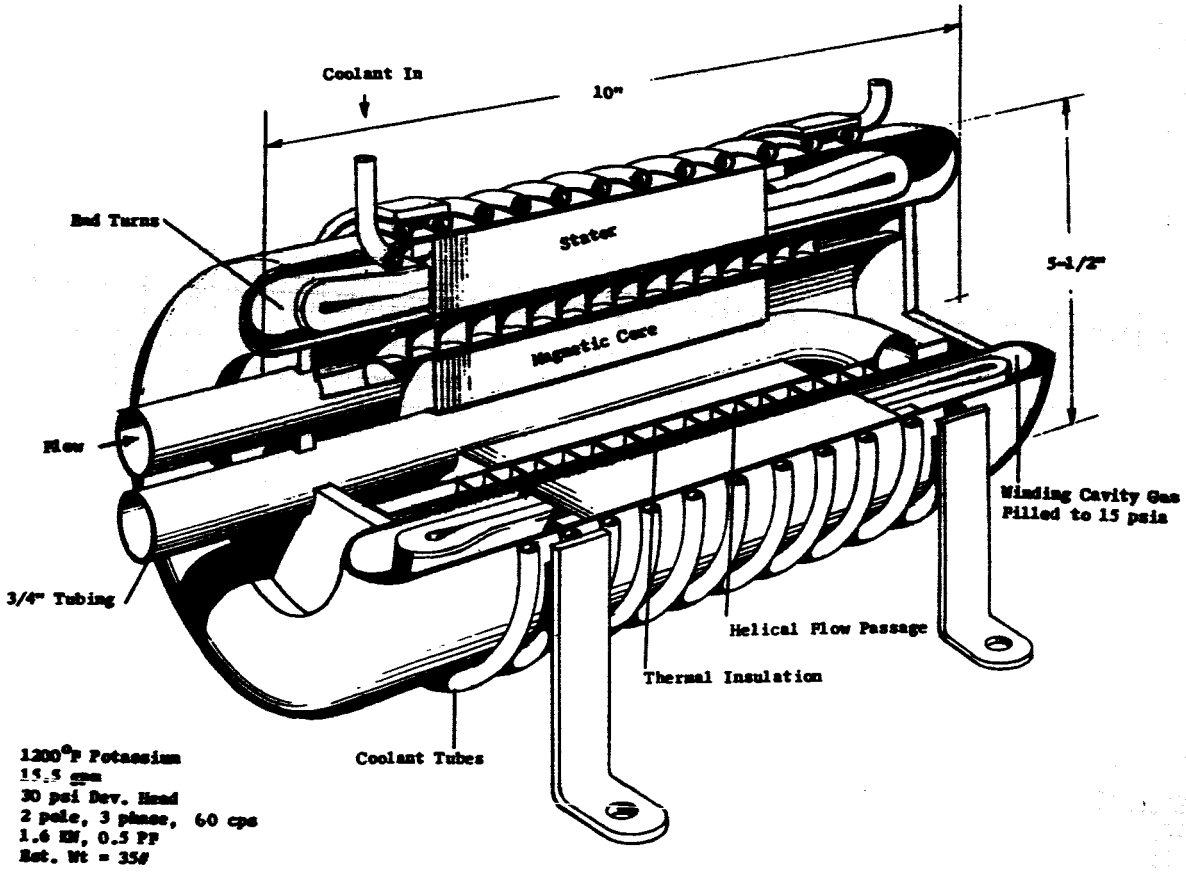

Figure VII-3

RADIATOR COOLANT PUMP TURBOELECTRIC SYSTEM

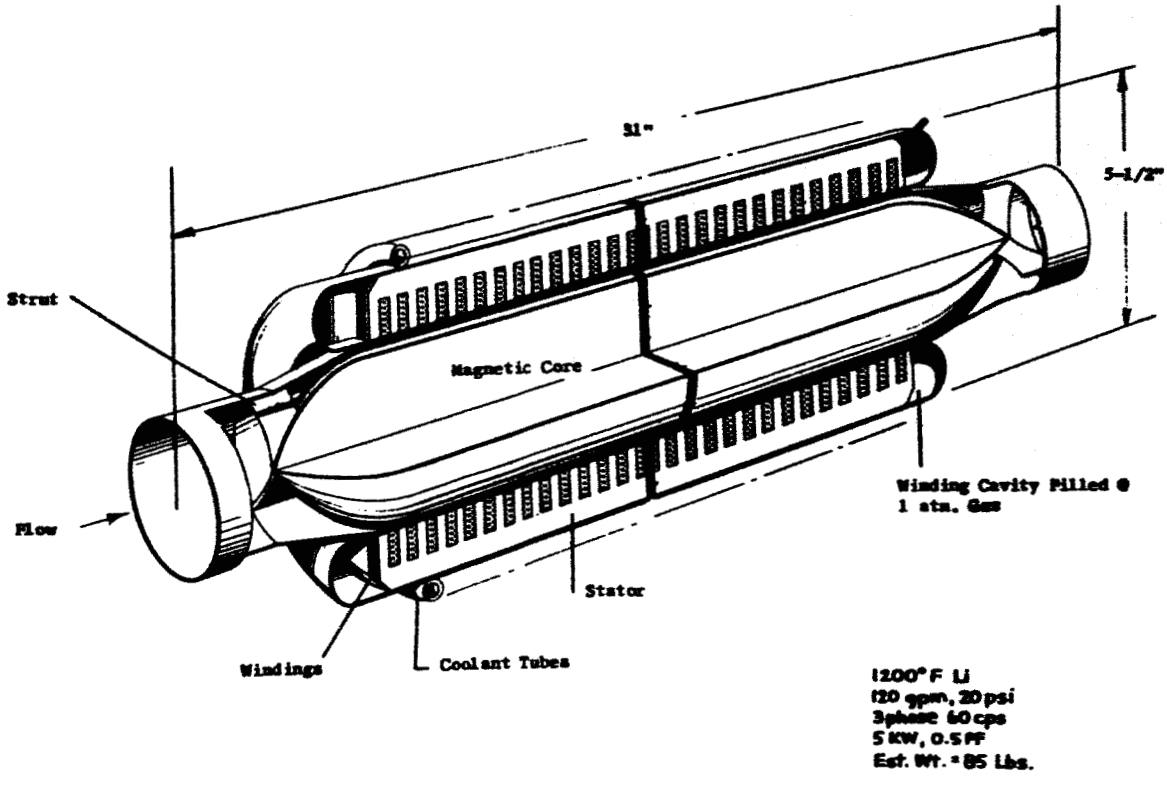

Figure VII-4

BOILER FEED PUMP TURBOELECTRIC SYSTEM

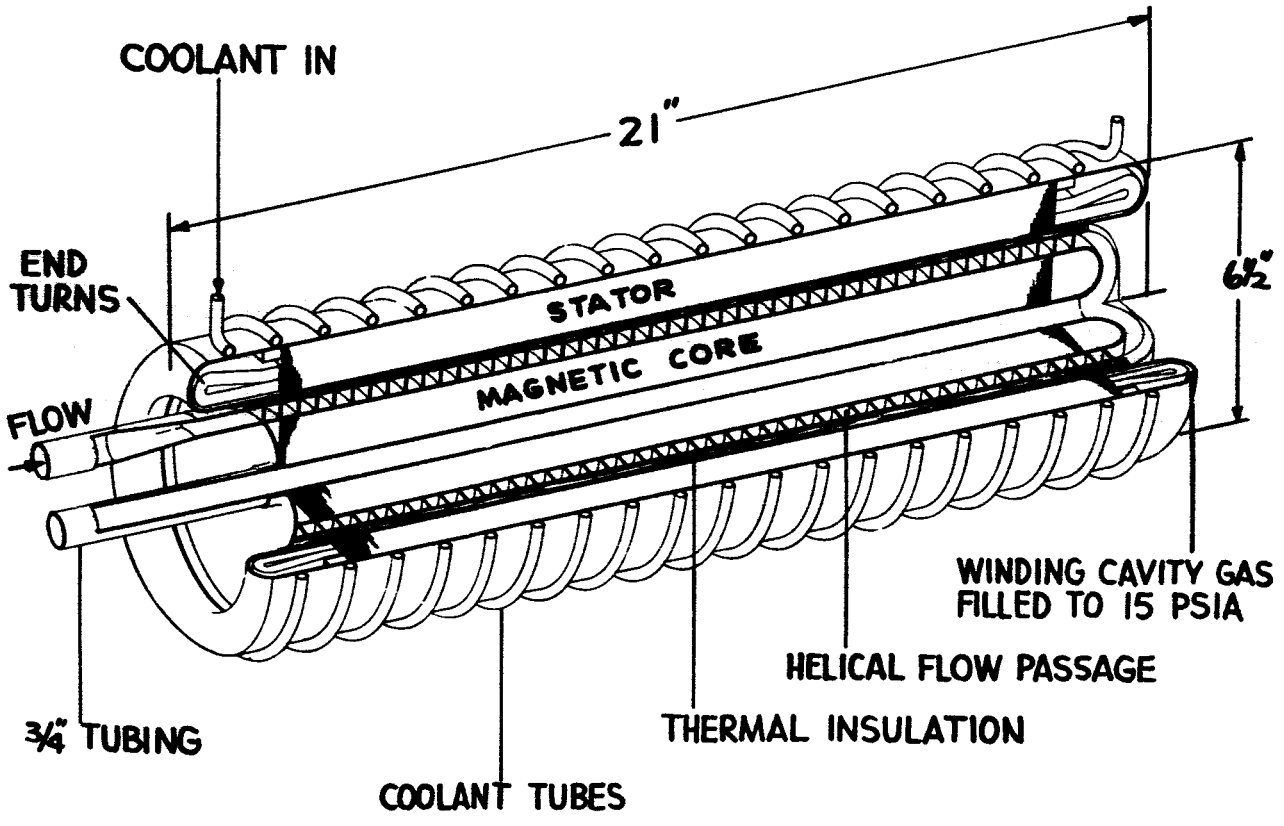

1200°F POTASSIUM
15.5 GPM
100 PSI DEV. HEAD
2 POLE, 3 PHASE, 60 CPS
5 KW, 0.5 PF
EST. WT. = 105 LBS.

Figure VII-5

C64031324